


Ratio of products of mixture gamma variates with applications to wireless communications systems

Hussien Al-Hmood¹  | Hamed Al-Raweshid²

¹ Electrical and Electronic Engineering (EEE) Department, College of Engineering, University of Thi-Qar, Nassiriyah, Thi-Qar, Iraq

² Electrical and Computer Engineering (ECE) Department, College of Engineering, Design and Physical Sciences, Brunel University, Uxbridge, London, UK

Correspondence

Hamed Al-Raweshid, Electrical and Computer Engineering (ECE) Department, College of Engineering, Design and Physical Sciences, Brunel University, Uxbridge UB8 3PH, London, UK.
Email: Hamed.Al-Raweshidy@brunel.ac.uk

Abstract

The fading scenario of many realistic wireless communication transmission systems, such as, multi-hop communications and spectrum sharing in cognitive radio networks (CRNs), can be modelled by the product and the ratio of the product of the random variables (RVs) of the channel distribution. However, there is no work has been investigated in the literature to provide unified statistics of the product and the ratio of the products that can be used for a wide range of non-composite and composite fading conditions. Accordingly, in this paper, the statistical properties, namely, probability density function (PDF), cumulative distribution function (CDF), and moment generating function (MGF) of the product and the ratio of the product of independent and non-identically distributed (i.n.d.) mixture Gamma (MG) RVs are derived. A MG distribution has been widely employed to approximate with high accuracy most of the conventional fading models, for example, Rayleigh, Nakagami- m , Nakagami- q (Hoyt), and Nakagami- n (Rician) as well as the generalised composite fading channels, such as, generalised- K (K_G), $\alpha - \mu$ /gamma, $\kappa - \mu$ /gamma, and $\eta - \mu$ /gamma. Hence, the derived PDF, CDF, and MGF are utilized for the Beaulieu-Xie and $\alpha - \lambda - \eta - \mu$ shadowed fading channels that have not been yet presented by the previous works due to mathematical intractability of their statistics. Thus, the equivalent parameters of a MG distribution for these channels are given. To this end, simple closed-form mathematically tractable expressions of the performance metrics are obtained. The derived statistics are applied to analyse the outage probability (OP), the average error probability for different modulation schemes, the effective rate (ER) of wireless communication systems and the average area under the receiver operating characteristics (AUC) curve of energy detection over cascaded fading channels. Moreover, the OP of the multi-hop communications systems with co-channel interference (CCI), both the lower bound of secure OP (SOP^L) and probability of non-zero secrecy capacity (PNSC) of the physical layer security (PLS), and the outage and delay-limited capacities of CRNs are studied via using the statistics of the ratio of the product of MG variates. A comparison between the numerical results and the Monte Carlo simulations is presented to verify the validation of our analysis.

1 | INTRODUCTION

The performance of several practical wireless communications systems can be analysed via using different approaches of fading conditions [1–10]. For example, the statistical properties of the product of the random variables (RVs) can be employed for cascaded fading channels, multihop transmission with non-regenerative relays [1], multi-antenna systems operating in the

presence of keyholes [3], and vehicle-to-vehicle (V2V) communications [5]. In addition, the performance of wireless communications systems in the presence of co-channel interference (CCI) [6], physical layer security (PLS) [7], spectrum sharing in cognitive radio networks [9], [10] can be investigated by the ratio of products of the variates.

Motivated by the above, many efforts have been devoted in the open technical literature to derive the distribution of the

This is an open access article under the terms of the [Creative Commons Attribution](https://creativecommons.org/licenses/by/4.0/) License, which permits use, distribution and reproduction in any medium, provided the original work is properly cited.

© 2021 The Authors. *IET Communications* published by John Wiley & Sons Ltd on behalf of The Institution of Engineering and Technology

product of RVs using different models. For instance, in [11], the statistical properties, namely, the probability density function (PDF), cumulative distribution function (CDF), and moment generating function (MGF), of the product of N independent and non-identically distributed (i.n.d.) Nakagami- m variates were derived. In [12], the PDF of the product of independent Rayleigh variates was approximated to be expressed in terms of the elementary functions, such as power and exponential. Simple approximate expressions for the PDF and CDF of the cascaded independent Rayleigh, generalised Gamma (GG), Nakagami- m , Gaussian, and Weibull fading channels were given in [13]. The statistical characterisations of the product of i.n.d. squared generalised- $K(K_G)$ variates were presented in [3] with applications to the outage probability (OP) and average bit error probability (ABEP) over cascaded fading channels.

On the other hand, several distributions of the ratio of products of RVs have been analysed by the previous works. For example, the performances of the maximal ratio combining (MRC) diversity reception and multi-carrier code-division multiple access (MC-CDMA) system in the presence of an interference were studied in [14] by using the statistics of independent and identically distributed (i.i.d.) exponential variates. In [15], the ratio of products of both Gamma and Weibull RVs were analysed. The cascaded Weibull distribution was reported in [16]. The distribution of some mathematical operations, such as, products and ratios, of arbitrary H -function variates that can be used as a unified representation for a large number of fading channels, was derived in [17].

Recently, the product of the RVs of Fisher-Snedecor \mathcal{F} [7], [9], generalised $\alpha - \mu, \kappa - \mu$, and $\eta - \mu$, [18–22], fluctuating two-ray (FTR) [23], and Beaulieu-Xie [24] distributions has been given a special attention by many research articles. This is because these distributions give better fitting to the practical data and provide various composite multipath/shadowing fading conditions. Moreover, they approximately include all the well-known classic fading channels, such as, Rayleigh, Nakagami- m , Rician, exponential distributions as special cases. Additionally, the $\alpha - \mu$ fading channel is used to model the non-linear environment of communication systems whereas the $\kappa - \mu$ and the $\eta - \mu$ fading channels are employed to represent the line-of-sight (LoS) and the non-LoS (NLoS) scenarios, respectively. Besides, the FTR distribution has been widely utilised to model the fading channel of the millimeter-wave (mmWave) communication systems. Hence, the statistics of i.n.d. cascaded Fisher-Snedecor \mathcal{F} fading channel which is composite of Nakagami- m /inverse Nakagami- m distributions, were studied in [7] and [9] in terms of the Meijer's G -function and applied in the analysis of the OP and ABEP of amplify-and-forward (AF)-relaying communication systems. The PDF, CDF, and MGF of the product of two i.n.d. $\alpha - \mu$ and $\kappa - \mu$ variates and their applications to double and composite fading channels were reported in [18] and [19], respectively. Two different expressions of the statistics of non-identical cascaded $\alpha - \mu$ fading channels were given in [20] and [21] in terms of the Fox's H -function (FHF) and utilised in the analysis of the OP and ABEP, and the average secrecy capacity (ASC), lower bound of secure outage probability (SOP^L) and probability of non-zero

secrecy capacity (PNSC) of the PLS, respectively. The product of two envelopes of $\alpha - \mu, \kappa - \mu$, and $\eta - \mu$ distributions were investigated in [22] via providing infinite series expressions and closed-form results in terms of the multivariate FHF. The distribution of the cascaded FTR variates with non-identical shaping parameters was investigated in [23]. The fundamental statistics of two i.n.d. Beaulieu-Xie RVs were provided in [24] in terms of double infinite series as well as Meijer's G -function.

On the other side, the statistics of the ratio of the product of FTR RVs with non-identical shaping indices was derived in [6] and utilised in the analysis of the OP of decode-and-forward (DF) relaying system. The statistics of the distribution of the ratio of the product of arbitrarily distributed N Fisher-Snedecor \mathcal{F} variates were presented in [7] and [9] with applications to PLS and CRNs, respectively. The ratio of two $\alpha - \mu$ RVs was given in [10] and used in the analysis of the outage and delay-limited capacities of the spectrum sharing in CRNs. The results of [10] was then extended by [25] to include multivariate of $\alpha - \mu$ distribution. Similar to the mathematical results of [22], the statistics of the ratio of two envelopes taken from $\alpha - \mu, \kappa - \mu$, and $\eta - \mu$ RVs were given in [26] and employed in the study of the PNSC of the PLS over different non-identical fading conditions of V2V communications. In [27], the product and the ratio of products of non-identically distributed GG variates were expressed in terms of the FHF.

Based on the previous studies that are summarised in Table 1, the statistical properties of the distributions of the product and the ratio of the products of an i.n.d. mixture Gamma (MG) variates that have not been yet investigated in the literature, are derived in this article. A MG distribution has been widely employed to approximate with high accuracy most of the conventional fading models, for example, Rayleigh, Nakagami- m , Nakagami- q (Hoyt), and Nakagami- n (Rician) as well as the generalised composite fading channels, such as, generalised- $K(K_G)$, $\alpha - \mu$ /gamma, $\kappa - \mu$ /gamma, and $\eta - \mu$ /gamma. To this end, unified simple closed-form mathematically tractable expressions of the fundamental statistics of the product and the ratio of the products that can be used for a wide range of non-composite and composite fading conditions of the realistic wireless communication transmission systems are obtained. Unlike the Gamma [14], \mathcal{G} [15], GG [27], and exponential-GG (EGG) [28] distributions, a MG distribution can give low mean-square error (MSE) and Kullback-Leibler (KL) divergence between the exact and the approximated models (please refer to [[30], Figures 1 and 2]). Additionally, the statistical characterisations of a MG distribution are simpler than that of a mixture of Gaussian (MoG) approach. Consequently, a MG distribution has been widely utilised as a highly accurate approximation for large numbers of fading models [30–37].

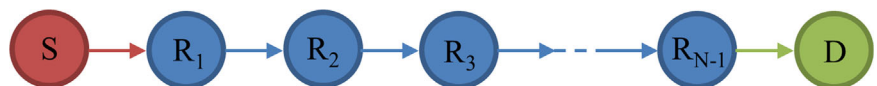
The main contributions of this paper are summarised as follows

- Deriving exact closed-form computationally tractable expressions of the PDF, CDF, and MGF of the distribution of the product of i.n.d. MG variates in terms of a single variable Meijer's G -function. To the best of the authors' knowledge,

TABLE 1 Survey of works related to product and ratio of products of RVs

Reference	Distribution	Product	Ratio of products	Exact/approximate	Performance metrics
[3]	K_G	✓	-	Exact	OP and ABEP
[6]	FTR	-	✓	Approximate	OP of DF relaying system
[7]	Fisher-Snedecor \mathcal{F}	✓	✓	Exact	OP, ABEP, SOP and PNSC
[9]	Fisher-Snedecor \mathcal{F}	✓	✓	Exact	Amount of fading (AoF), ACC, Channel quality estimation index (CQEI), OP, and ABEP of AF system, and Capacity in CRNs
[10]	$\alpha - \mu$	-	✓	Exact	Capacity in CRNs
[11]	Nakagami- m	✓	-	Exact	OP and ABEP
[12]	Rayleigh	✓	-	Approximate	ABEP
[13]	Rayleigh, GG, Nakagami- m , Gaussian, and Weibull	✓	-	Approximate	OP and ABEP
[14]	Exponential	-	✓	Exact	OP and ABEP
[15]	Gamma-Weibull	✓	✓	Exact	OP and ABEP
[16]	Weibull	✓	-	Exact	-
[17]	H -Function	✓	✓	Exact	-
[18]	Two $\alpha - \mu$	✓	-	Exact	OP and ABEP
[19]	Two $\kappa - \mu$	✓	-	Exact	OP and ABEP
[20]	$\alpha - \mu$	✓	-	Exact	OP and ABEP
[21]	$\alpha - \mu$	✓	-	Exact	ASC, SOP, and SOP^L
[22]	Two $\alpha - \mu, \kappa - \mu$, and $\eta - \mu$	✓	-	Exact	OP and ABEP
[23]	FTR	✓	-	Approximate	OP and ABEP
[24]	Two Beaulieu-Xie	✓	-	Approximate	OP and ACC
[25]	$\alpha - \mu$	-	✓	Exact	OP and ABEP
[26]	Two $\alpha - \mu, \kappa - \mu$, and $\eta - \mu$	-	✓	Exact	OP and ABEP
[27]	GG	✓	✓	Exact	-

FIGURE 1 Cascaded fading channels constructed by AF-relay nodes [9]



these unified statistics have not been yet achieved in the open technical literature.

- Based on the above results, novel statistical properties of the ratio of the product of i.n.d. MG variates are provided.

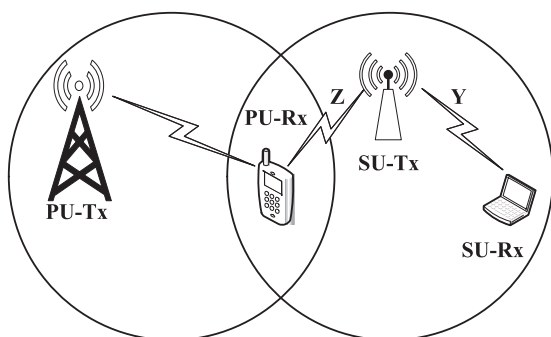


FIGURE 2 System model of spectrum sharing in CRNs [9]

- The equivalent parameters of a MG distribution for Beaulieu-Xie [38] and $\alpha - \lambda - \eta - \mu$ shadowed fading channels [39] that are not available in the open literature, are derived. It is worth mentioning that the statistics of these fading channels can not be obtained in exact closed-form due to including the PDF of a single RV on the modified Bessel function of the first kind. Moreover, the using of an infinite series of the modified Bessel function would lead to basic statistics in terms of the multiple infinite series that are converged slowly and unsteadily. These observations were presented in [24] where the PDF, CDF, and MGF of the products of two Beaulieu-Xie RVs were included double infinite series.
- Capitalising on the above statistics, the OP, ABEP, average symbol error probability (ASEP) for different modulation schemes, and the effective rate (ER) of communications systems and the average area under the receiver operating characteristics (AUC) of energy detection (ED) over non-identical cascaded fading channels are given in closed-form

TABLE 2 Survey of works related to mixture gamma distribution

Reference	Channel model	Applications	Evaluation tools	Performance metrics
[30]	Gamma-lognormal (GL), K_G , K , Rician, Hoyt, $\kappa - \mu$, $\eta - \mu$, Nakagami- m , and Rayleigh	Wireless communication systems and energy detection	PDF, CDF, and MGF	OP, ACC, ASEP, ADP, and AUC
[31]	Composite of $\kappa - \mu$ /gamma, $\eta - \mu$ /gamma, and $\alpha - \mu$ /gamma	Energy detection	PDF	ADP and AUC
[32]	Composite of $\alpha - \lambda - \eta - \mu$ /gamma	Wireless communication systems	PDF and CDF	ACC
[33]	Composite of $\alpha - \eta - \mu$ /gamma	Wireless communication systems	PDF	EC
[34]	K_G	PLS	PDF and CDF	ASC, SOP, and SOP ^L
[35]	$\alpha - \mu$	PLS	PDF and CDF	ASC, SOP, and SOP ^L
[36]	K_G	MRC and SC with i.i.d. branches	PDF, CDF, and MGF	OP, ABEP, and ACC
[37]	$\eta - \mu$ /gamma	MRC and SC with i.n.d. branches	PDF, CDF, and MGF	OP, ABEP, and ACC

expressions. To the best of the authors knowledge, both the ER and average AUC of ED over cascaded fading channels have not been yet investigated in the literature.

- Utilising the CDF of the ratio of products to analyse the OP of multihop communications systems with DF relaying protocol and subject to multiple interferes as well as the SOP^L, and PNSC of the PLS. In contrast to [40] in which the SOP^L and PNSC over Beaulieu–Xie fading are expressed in terms of infinite series, our derived results are given in simple closed-form expressions. Additionally, the outage and delay-limited capacities of the spectrum sharing in CRNs are studied for different transmission scenarios.

Organization: Section 2 provides some related works to a MG distribution based fading channel model of wireless communications systems. In Section 3.1, the statistical properties of the product of MG variates are derived, whereas in Section 3.2, the statistics of the ratio of products of MG RVs are given. The equivalent parameters of a MG distribution for Beaulieu–Xie and $\alpha - \lambda - \eta - \mu$ shadowed fading are provided in Section 4. Based on the results of Section 3.1 and Section 3.2, some performance measures are derived in Section 5 and Section 6, respectively. The numerical results are presented in Section 7. Finally, some conclusions are highlighted in Section 8.

2 | RELATED WORKS TO MG DISTRIBUTION

Motivated by the advantages of a MG model that have been mentioned previously, this distribution has been used by several efforts to represent the fading channels of the wireless communication systems. However, there is no work has been investigated in the literature to provide unified statistics of the product and the ratio of the products that can be used for a wide range of non-composite and composite fading conditions. Accordingly, in this paper, the statistical properties of the product and the ratio of the product of i.n.d. MG RVs are derived.

Table 2 summarises some of the most relevant works related to using a MG distribution in modelling a fading channel,

applications in the realistic wireless communication systems, evaluation tools, and performance metrics. For instance, in [30], the OP, ABEP, average channel capacity (ACC), and performance of ED over Nakagami- m , $\kappa - \mu$, and $\eta - \mu$ and other fading channels were analysed. The average detection probability (ADP) and average AUC curve of ED over $\alpha - \mu$ /Gamma, $\kappa - \mu$ /Gamma, and $\eta - \mu$ /Gamma fading channels were investigated in [31]. Furthermore, unified frameworks of the channel capacity under different transmission protocols and the ER of wireless communications systems over $\alpha - \eta - \mu$ /Gamma fading conditions were presented in [32] and [33], respectively. The performance of the PLS over MG distribution based channel model of both the main and wire-tap channels were analysed in [34] and [35]. The sum and the maximum of i.i.d. K_G and i.n.d. $\eta - \mu$ /gamma fading channels were derived in [36] and [37], respectively, using a MG distribution with applications to the selection combining (SC) and the MRC diversity receptions.

3 | PRODUCT AND RATIO OF PRODUCTS OF MG VARIATES

The PDF of the instantaneous signal-to-noise ratio (SNR) at i^{th} path, γ_i , using a MG distribution is expressed as [[30], equation (1)]

$$f_{\gamma_i}(\gamma) = \sum_{l_i=1}^{L_i} \sigma_{l_i} \gamma^{\beta_{l_i}-1} e^{-\zeta_{l_i} \gamma}, \quad (1)$$

where L_i stands for the number of terms of l^{th} Gamma component with parameters σ_{l_i} , β_{l_i} , and ζ_{l_i} . According to [30], the minimum number of terms, L_i , that can provide a good matching between the approximate and exact distributions can be computed by using the MSE between the PDF of these distributions.

3.1 | Product of i.n.d. MG variates

Theorem 1. Let $Y \triangleq \prod_{i=1}^N \gamma_i$, where $\gamma_i \sim MG(L_i, \sigma_{l_i}, \beta_{l_i}, \zeta_{l_i})$ for $i = 1, \dots, N$ are i.n.d. MG-distributed RVs. Then, the PDF, CDF,

and MGF of Y are, respectively, given by

$$f_Y(y) = \sum_{l_1=1}^{L_1} \cdots \sum_{l_N=1}^{L_N} \Phi_N G_{0,N}^{N,0} \left[\frac{\Xi_N}{y} \middle| (\beta_{l_i} - 1)_{i=1:N} \right], \quad (2)$$

$$F_Y(y) = \sum_{l_1=1}^{L_1} \cdots \sum_{l_N=1}^{L_N} \frac{\Phi_N}{y^{N+1}} G_{1,N+1}^{N,1} \left[\frac{\Xi_N}{y} \middle| (\beta_{l_i} - 1)_{i=1:N}, -1 \right], \quad (3)$$

$$\mathcal{M}_Y(s) = \sum_{l_1=1}^{L_1} \cdots \sum_{l_N=1}^{L_N} \frac{\Phi_N}{s} G_{1,N}^{N,1} \left[\frac{\Xi_N}{s} \middle| (\beta_{l_i} - 1)_{i=1:N} \right], \quad (4)$$

where $\Phi_N = \prod_{i=1}^N \frac{\sigma_{l_i}}{\zeta_{l_i}^{\beta_{l_i}-1}}$, $\Xi_N = \prod_{i=1}^N \zeta_{l_i}$ and $G_{p,q}^{a,b}[\cdot]$ is the Meijer's G -function defined in [[41], equation (1.112)].

Proof. The Mellin transform of Y , $\mathbf{M}_Y(n)$, can be expressed as

$$\mathbf{M}_Y(n) = \prod_{i=1}^N \mathbf{M}_{\gamma_i}(n). \quad (5)$$

where $\mathbf{M}_{\gamma_i}(n)$ can be evaluated by [[41], equation (2.1)]

$$\mathbf{M}_{\gamma_i}(n) = \int_0^\infty \gamma^{n-1} f_{\gamma_i}(\gamma) d\gamma. \quad (6)$$

Substituting (1) into (6) and using [[42], equation (3.381.4)], this yields

$$\mathbf{M}_{\gamma_i}(n) = \sum_{l_i=1}^{L_i} \sigma_{l_i} \zeta_{l_i}^{1-n-\beta_{l_i}} \Gamma(\beta_{l_i} - 1 + n). \quad (7)$$

where $\Gamma(\cdot)$ is the Gamma function [[42], equation (8.310.1)].

Now, plugging (7) in (5) to obtain

$$\mathbf{M}_Y(n) = \sum_{l_1=1}^{L_1} \cdots \sum_{l_N=1}^{L_N} \Phi_N \Xi_N^{-n} \prod_{i=1}^N \Gamma(\beta_{l_i} - 1 + n). \quad (8)$$

Recalling the inverse Mellin transform [[43], equation (1.20)] for (8), we have

$$f_Y(y) = \sum_{l_1=1}^{L_1} \cdots \sum_{l_N=1}^{L_N} \Phi_N \times \frac{1}{2\pi i} \int_{\mathcal{L}} \left(\prod_{i=1}^N \Gamma(\beta_{l_i} - 1 + t) \right) (\Xi_N)^{-t} dt. \quad (9)$$

where $\mathbf{i} = \sqrt{-1}$, and \mathcal{L} is the suitable contours in the t -plane from $\varrho - \mathbf{i}\infty$ to $\varrho + \mathbf{i}\infty$ with ϱ is a constant value.

With the help of [[41], equation (1.112)], (9) can be written as in (2) which completes the proof of the PDF.

The CDF of Y can be deduced after substituting (2) into $F_Y(y) = \int_0^y f_Y(y) dy$ and invoking [[41], equation (2.53)].

The MGF of Y can be obtained via inserting (2) in $\mathcal{M}_Y(s) = \int_0^\infty e^{-sy} f_Y(y) dy$ and using [[41], equation (2.29)] which finishes the proof. \square

3.2 | Ratio of products of i.n.d. MG variates

Theorem 2. Assume $X \triangleq \frac{Y}{Z}$ where $Y = \prod_{i=1}^N \gamma_{1,i}$ and $Z = \prod_{j=1}^M \gamma_{2,j}$ where $\gamma_{1,i} \sim MG(L_{1,i}, \sigma_{l_{1,i}}, \beta_{l_{1,i}}, \zeta_{l_{1,i}})$ for $i = 1, \dots, N$ and $\gamma_{2,j} \sim MG(L_{2,j}, \sigma_{l_{2,j}}, \beta_{l_{2,j}}, \zeta_{l_{2,j}})$ for $j = 1, \dots, M$ are i.n.d. MG-distributed RVs. Accordingly, the PDF, CDF, and MGF of X are, respectively, deduced as

$$f_X(x) = \sum_{l_i=1}^{L_i} \sum_{l_j=1}^{L_j} \frac{\Phi_N \Phi_M}{\Xi_M^2} \times G_{M,N}^{N,M} \left[\frac{\Xi_N}{\Xi_M x} \middle| (\beta_{l_j})_{j=1:M}, (\beta_{l_i} - 1)_{i=1:N} \right], \quad (10)$$

$$F_X(x) = \sum_{l_i=1}^{L_i} \sum_{l_j=1}^{L_j} \frac{\Phi_N \Phi_M}{\Xi_M^2} \times G_{M+1,N+1}^{N,M+1} \left[\frac{\Xi_N}{\Xi_M x} \middle| (\beta_{l_j})_{j=1:M}, 0, (\beta_{l_i} - 1)_{i=1:N}, -1 \right], \quad (11)$$

$$\mathcal{M}_X(s) = \sum_{l_i=1}^{L_i} \sum_{l_j=1}^{L_j} \frac{\Phi_N \Phi_M}{\Xi_M^2 s} \times G_{M+1,N}^{N,M+1} \left[\frac{\Xi_N}{s \Xi_M} \middle| (\beta_{l_j})_{j=1:M}, 0, (\beta_{l_i} - 1)_{i=1:N} \right], \quad (12)$$

Proof. To compute the Mellin transform for both Y and Z , the methodology that is given in Theorem 1 is used. Thereafter, plugging the result in $\mathbf{M}_X(n) = \mathbf{M}_Y(n) \mathbf{M}_Z(2-n)$ to obtain

$$\mathbf{M}_X(n) = \sum_{l_i=1}^{L_i} \Phi_N \Xi_N^{-n} \left(\prod_{i=1}^N \Gamma(\beta_{l_i} - 1 + n) \right) \sum_{l_j=1}^{L_j} \Phi_M \Xi_M^{-(2-n)} \left(\prod_{j=1}^M \Gamma(\beta_{l_j} + 1 - n) \right). \quad (13)$$

Substituting (13) into [[43], equation (1.21)], the PDF of X can be expressed as

$$f_X(x) = \sum_{l_i=1}^{L_i} \sum_{l_j=1}^{L_j} \frac{\Phi_N \Phi_M}{\Xi_M^2} \frac{1}{2\pi i} \int_{\mathcal{L}} \left(\frac{\Xi_N}{\Xi_M x} \right)^{-t} \left(\prod_{i=1}^N \Gamma(\beta_{l_i} - 1 + n) \right) \left(\prod_{j=1}^M \Gamma(\beta_{l_j} + 1 - n) \right) dt. \quad (14)$$

With the aid of the definition of Meijer's G -function [[41], equation (1.112)], (14) is obtained as shown in (10) and the proof is accomplished.

Following the similar steps of deriving (3) and (4) that are provided in Theorem 1, the CDF and the MGF of X can be deduced as given in (11) and (12), respectively, which completes the proof. \square

4 | MODELING OF GENERALIZED COMPOSITE FADING CHANNELS USING A MG DISTRIBUTION

4.1 | Beaulieu–Xie fading channels

The Beaulieu–Xie fading model is proposed as a simple representation for multiple specular and diffuse scatter components via introducing a special scale for the non-central chi-distribution [38]. Moreover, this model unifies the non-central chi, $\kappa - \mu$, and generalized Rician distributions where the relationship between the latter and Beaulieu–Xie distributions is the same as that between the Nakagami- m and Rayleigh models. Additionally, the Beaulieu–Xie distribution is related to the Nakagami- m model in a similar relationship that is between the Rician and Rayleigh fading models [38].

The PDF of $\gamma_i, f_{\gamma_i}(\gamma)$, over Beaulieu–Xie fading channel can be derived after employing [[38], equation (4)] and performing simple change of variables. Thus, this yields

$$f_{\gamma_i}(\gamma) = \frac{2^{\frac{m_i-1}{2}} m_i^{\frac{m_i+1}{2}} e^{-\frac{\lambda_i^2}{2}} \gamma^{\frac{m_i-1}{2}} e^{-\frac{m_i}{\bar{\gamma}_i} \gamma}}{\lambda_i^{m_i-1} \bar{\gamma}_i^{\frac{m_i+1}{2}}} \times I_{m_i-1} \left(\lambda_i \sqrt{\frac{2m_i \gamma}{\bar{\gamma}_i}} \right), \quad (15)$$

where $\bar{\gamma}_i$ is the average SNR, m_i is the fading parameter, λ_i controls the location and the height of the PDF, and $I_{m_i-1}(\cdot)$ is the modified Bessel function of the first kind and $m_i - 1$ order. When $m_i = 1$, the Beaulieu–Xie fading model reduces to Rician distribution with factor $K_i = \lambda_i/\Omega_i$ where Ω_i controls the spread of the PDF whereas the Rayleigh fading is obtained after plugging $m_i = 1$ and $K_i = 0$.

With the aid of the identity [[42], equation (8.445)], the modified Bessel function of (15) can be written as

$$I_{m_i-1} \left(\lambda_i \sqrt{\frac{2m_i \gamma}{\bar{\gamma}_i}} \right) = \sum_{l_i=1}^{\infty} \frac{1}{\Gamma(l_i)\Gamma(m_i + l_i - 1)} \left(\lambda_i \sqrt{\frac{2m_i \gamma}{\bar{\gamma}_i}} \right)^{2l_i+m_i-3}. \quad (16)$$

Plugging (16) in (15), we have

$$f_{\gamma_i}(\gamma) = \sum_{l_i=1}^{\infty} \frac{\lambda_i^{2(l_i-1)} e^{-\frac{\lambda_i^2}{2}} \left(\frac{2m_i}{\bar{\gamma}_i} \right)^{m_i+l_i-2}}{\Gamma(l_i)\Gamma(m_i + l_i - 1)} \gamma^{m_i+l_i-2} e^{-\frac{m_i}{\bar{\gamma}_i} \gamma}. \quad (17)$$

It can be noted that the infinite series of (17) can be approximated to the number of terms, L_i , that satisfies the required accuracy of the MSE. Accordingly, by matching the PDF of (17) with that of (15), the equivalent parameters of a MG for the Beaulieu–Xie fading channel are expressed as

$$\beta_{l_i} = m_i + l_i - 1, \quad \sigma_{l_i} = \frac{\theta_{l_i}}{\sum_{j_i=1}^{L_i} \theta_{j_i} \Gamma(\beta_{j_i}) \zeta_{j_i}^{-\beta_{j_i}}}$$

$$\zeta_{l_i} = \frac{m_i}{\bar{\gamma}_i}, \quad \theta_{l_i} = \frac{\lambda_i^{2(l_i-1)} e^{-\frac{\lambda_i^2}{2}} \left(\frac{2m_i}{\bar{\gamma}_i} \right)^{m_i+l_i-2}}{\Gamma(l_i)\Gamma(m_i + l_i - 1)}. \quad (18)$$

4.2 | $\alpha - \lambda - \eta - \mu$ Shadowed fading channels

The $\alpha - \lambda - \eta - \mu$ shadowed fading channel is a composite model of $\alpha - \lambda - \eta - \mu$ and Nakagami- m distributions. The $\alpha - \lambda - \eta - \mu$ was proposed by [39] as a generalised distribution that unifies the $\alpha - \mu, \lambda - \mu$, and $\eta - \mu$ fading models. Hence, this fading model can be employed to represent the non-linear medium and the non-line-of-sight (NLoS) environment of the wireless communications. Furthermore, the $\alpha - \lambda - \eta - \mu$ shadowed can be used to model a wide range of composite multipath/shadowed fading conditions, such as, $\alpha - \mu$ /Nakagami- $m, \lambda - \mu$ /Nakagami- m , and $\eta - \mu$ /Nakagami- m as explained in Table 3. However, the PDF of the $\alpha - \lambda - \eta - \mu$ distribution is included a modified Bessel function which would lead to express the results in terms of non-analytical mathematically complicated functions or include an infinite series. Hence, a MG distribution is used in this effort to approximate the PDF of the composite $\alpha - \lambda - \eta - \mu$ /Nakagami- m fading channel.

The PDF of $\gamma_i, f_{\gamma_i}(\gamma)$, over $\alpha - \lambda - \eta - \mu$ fading channel is given as [[39], equation (10)]

$$f_{\gamma_i}(\gamma) = \psi_i \gamma^{\phi_i-1} e^{-\rho_i \gamma^{\frac{\alpha_i}{2}}} I_{\mu_i-\frac{1}{2}} \left(\vartheta_i \gamma^{\frac{\alpha_i}{2}} \right). \quad (19)$$

where

$$\psi_i = \frac{\sqrt{\pi} \alpha_i (\mu_i (1 + \eta_i^{-1}))^{\mu_i + \frac{1}{2}} \left(\frac{\eta_i}{1 - \lambda_i^2} \right)^{\mu_i}}{\Gamma(\mu_i) a_i^{\mu_i - \frac{1}{2}} \bar{\gamma}_i^{\frac{\alpha_i}{2} (\mu_i + \frac{1}{2})}}$$

TABLE 3 Special cases of $\alpha - \lambda - \eta - \mu$ shadowed distribution

Fading distribution	Format 1	Format 2
$\alpha - \eta - \mu$ shadowed	$\underline{\alpha} = \alpha, \underline{\mu} = \mu, \underline{m} = m, 0 < \underline{\eta} < \infty, \underline{\lambda} \rightarrow 0$ $\underline{\alpha} = \alpha, \underline{\mu} = 2\mu, \underline{m} = m, 0 < \underline{\eta} < \infty, \underline{\lambda} \rightarrow 1$	$\underline{\alpha} = \alpha, \underline{\mu} = \mu, \underline{m} = m, -1 < \underline{\eta} < 1, \underline{\lambda} \rightarrow 0$ $\underline{\alpha} = \alpha, \underline{\mu} = 2\mu, \underline{m} = m, -1 < \underline{\eta} < 1, \underline{\lambda} \rightarrow 1$
$\alpha - \lambda - \mu$ shadowed	$\underline{\alpha} = \alpha, \underline{\mu} = \mu, \underline{m} = m, \underline{\eta} \rightarrow 1, \underline{\lambda} = \lambda$ $\underline{\alpha} = \alpha, \underline{\mu} = 2\mu, \underline{m} = m, \underline{\eta} \rightarrow 0 \text{ or } \underline{\eta} \rightarrow \infty, \underline{\lambda} = \lambda$	$\underline{\alpha} = \alpha, \underline{\mu} = \mu, \underline{m} = m, \underline{\eta} \rightarrow 0, \underline{\lambda} = \lambda$ $\underline{\alpha} = \alpha, \underline{\mu} = 2\mu, \underline{m} = m, \underline{\eta} \rightarrow 1, \underline{\lambda} = \lambda$
$\lambda - \eta - \mu$ shadowed	$\underline{\alpha} = 2, \underline{\mu} = \mu, \underline{m} = m, 0 < \underline{\eta} < \infty, \underline{\lambda} = \lambda$	$\underline{\alpha} = 2, \underline{\mu} = \mu, \underline{m} = m, -1 < \underline{\eta} < 1, \underline{\lambda} = \lambda$
$\alpha - \mu$ shadowed	$\underline{\alpha} = \alpha, \underline{\mu} = \mu, \underline{m} = m, \underline{\eta} \rightarrow 1, \underline{\lambda} \rightarrow 0$ $\underline{\alpha} = \alpha, \underline{\mu} = 2\mu, \underline{m} = m, \underline{\eta} \rightarrow 0 \text{ or } \underline{\eta} \rightarrow \infty, \underline{\lambda} \rightarrow 1$	$\underline{\alpha} = \alpha, \underline{\mu} = \mu, \underline{m} = m, \underline{\eta} \rightarrow \pm 1, \underline{\lambda} \rightarrow 0$ $\underline{\alpha} = \alpha, \underline{\mu} = 2\mu, \underline{m} = m, \underline{\eta} \rightarrow 0, \underline{\lambda} \rightarrow 1$
$\eta - \mu$ shadowed	$\underline{\alpha} = 2, \underline{\mu} = \mu, \underline{m} = m, 0 < \underline{\eta} < \infty, \underline{\lambda} \rightarrow 0$ $\underline{\alpha} = 2, \underline{\mu} = 2\mu, \underline{m} = m, 0 < \underline{\eta} < \infty, \underline{\lambda} \rightarrow 1$	$\underline{\alpha} = 2, \underline{\mu} = \mu, \underline{m} = m, -1 < \underline{\eta} < 1, \underline{\lambda} \rightarrow 0$ $\underline{\alpha} = 2, \underline{\mu} = 2\mu, \underline{m} = m, -1 < \underline{\eta} < 1, \underline{\lambda} \rightarrow 1$
$\lambda - \mu$ shadowed	$\underline{\alpha} = 2, \underline{\mu} = \mu, \underline{m} = m, \underline{\eta} \rightarrow 1, \underline{\lambda} = \lambda$ $\underline{\alpha} = 2, \underline{\mu} = 2\mu, \underline{m} = m, \underline{\eta} \rightarrow 0 \text{ or } \underline{\eta} \rightarrow \infty, \underline{\lambda} = \lambda$	$\underline{\alpha} = 2, \underline{\mu} = \mu, \underline{m} = m, \underline{\eta} \rightarrow \pm 1, \underline{\lambda} = \lambda$ $\underline{\alpha} = 2, \underline{\mu} = 2\mu, \underline{m} = m, \underline{\eta} \rightarrow 0, \underline{\lambda} = \lambda$
One-sided Gaussian shadowed	$\underline{\alpha} = 2, \underline{\mu} = 0.5, \underline{m} = m, \underline{\eta} \rightarrow 1, \underline{\lambda} \rightarrow 0$ $\underline{\alpha} = 2, \underline{\mu} = 1, \underline{m} = m, \underline{\eta} \rightarrow 0 \text{ or } \underline{\eta} \rightarrow \infty, \underline{\lambda} \rightarrow 1$	$\underline{\alpha} = 2, \underline{\mu} = 0.5, \underline{m} = m, \underline{\eta} \rightarrow \pm 1, \underline{\lambda} \rightarrow 0$ $\underline{\alpha} = 2, \underline{\mu} = 1, \underline{m} = m, \underline{\eta} \rightarrow 0, \underline{\lambda} \rightarrow 1$
Hoyt shadowed	$\underline{\alpha} = 2, \underline{\mu} = 0.5, \underline{m} = m, \underline{\eta} = q^2, \underline{\lambda} \rightarrow 0$ $\underline{\alpha} = 2, \underline{\mu} = 1, \underline{m} = m, \underline{\eta} = q^2, \underline{\lambda} \rightarrow 1$	$\underline{\alpha} = 2, \underline{\mu} = 0.5, \underline{m} = m, \underline{\eta} = \frac{1-q^2}{1+q^2}, \underline{\lambda} \rightarrow 0$ $\underline{\alpha} = 2, \underline{\mu} = 1, \underline{m} = m, \underline{\eta} = \frac{1-q^2}{1+q^2}, \underline{\lambda} \rightarrow 1$
Weibull shadowed	$\underline{\alpha} = k, \underline{\mu} = 0.5, \underline{m} = m, \underline{\eta} \rightarrow 1, \underline{\lambda} \rightarrow 0$ $\underline{\alpha} = k, \underline{\mu} = 1, \underline{m} = m, \underline{\eta} \rightarrow 0 \text{ or } \underline{\eta} \rightarrow \infty, \underline{\lambda} \rightarrow 1$	$\underline{\alpha} = k, \underline{\mu} = 0.5, \underline{m} = m, \underline{\eta} \rightarrow \pm 1, \underline{\lambda} \rightarrow 0$ $\underline{\alpha} = k, \underline{\mu} = 1, \underline{m} = m, \underline{\eta} \rightarrow 0, \underline{\lambda} \rightarrow 1$
Negative exponential shadowed	$\underline{\alpha} = 1, \underline{\mu} = 0.5, \underline{m} = m, \underline{\eta} \rightarrow 1, \underline{\lambda} \rightarrow 0$ $\underline{\alpha} = 1, \underline{\mu} = 1, \underline{m} = m, \underline{\eta} \rightarrow 0 \text{ or } \underline{\eta} \rightarrow \infty, \underline{\lambda} \rightarrow 1$	$\underline{\alpha} = 1, \underline{\mu} = 0.5, \underline{m} = m, \underline{\eta} \rightarrow \pm 1, \underline{\lambda} \rightarrow 0$ $\underline{\alpha} = 1, \underline{\mu} = 1, \underline{m} = m, \underline{\eta} \rightarrow 0, \underline{\lambda} \rightarrow 1$
Gamma shadowed	$\underline{\alpha} = 1, \underline{\mu} = a, \underline{m} = m, \underline{\eta} \rightarrow 1, \underline{\lambda} \rightarrow 0$ $\underline{\alpha} = 1, \underline{\mu} = 2a, \underline{m} = m, \underline{\eta} \rightarrow 0 \text{ or } \underline{\eta} \rightarrow \infty, \underline{\lambda} \rightarrow 1$ $\underline{\alpha} = 2, \underline{\mu} = m, \underline{m} = m, \underline{\eta} \rightarrow \infty \text{ or } \underline{\eta} \rightarrow 0, \underline{\lambda} \rightarrow 0$	$\underline{\alpha} = 1, \underline{\mu} = a, \underline{m} = m, \underline{\eta} \rightarrow \pm 1, \underline{\lambda} \rightarrow 0$ $\underline{\alpha} = 1, \underline{\mu} = 2a, \underline{m} = m, \underline{\eta} \rightarrow 0, \underline{\lambda} \rightarrow 1$ $\underline{\alpha} = 2, \underline{\mu} = m, \underline{m} = m, \underline{\eta} \rightarrow \pm 1, \underline{\lambda} \rightarrow 0$
K_G	$\underline{\alpha} = 2, \underline{\mu} = 2m, \underline{m} = m, \underline{\eta} \rightarrow \infty \text{ or } \underline{\eta} \rightarrow 0, \underline{\lambda} \rightarrow 1$ $\underline{\alpha} = 2, \underline{\mu} = 0.5m, \underline{m} = m, \underline{\eta} \rightarrow 1, \underline{\lambda} \rightarrow 0$ $\underline{\alpha} = 2, \underline{\mu} = m, \underline{m} = m, \underline{\eta} \rightarrow 1, \underline{\lambda} \rightarrow 1$	$\underline{\alpha} = 2, \underline{\mu} = 2m, \underline{m} = m, \underline{\eta} \rightarrow \pm 1, \underline{\lambda} \rightarrow 1$ $\underline{\alpha} = 2, \underline{\mu} = 0.5m, \underline{m} = m, \underline{\eta} \rightarrow 0, \underline{\lambda} \rightarrow 0$ $\underline{\alpha} = 2, \underline{\mu} = m, \underline{m} = m, \underline{\eta} \rightarrow 0, \underline{\lambda} \rightarrow 1$
K	K_G with $m = 1$	K_G with $m = 1$
$\alpha - \eta - \mu$	$\alpha - \eta - \mu$ shadowed with $\underline{m} \rightarrow \infty$	$\alpha - \eta - \mu$ shadowed with $\underline{m} \rightarrow \infty$
$\alpha - \lambda - \mu$	$\alpha - \lambda - \mu$ shadowed with $\underline{m} \rightarrow \infty$	$\alpha - \lambda - \mu$ shadowed with $\underline{m} \rightarrow \infty$
$\lambda - \eta - \mu$	$\lambda - \eta - \mu$ shadowed with $\underline{m} \rightarrow \infty$	$\lambda - \eta - \mu$ shadowed with $\underline{m} \rightarrow \infty$
$\alpha - \mu$	$\alpha - \mu$ shadowed with $\underline{m} \rightarrow \infty$	$\alpha - \mu$ shadowed with $\underline{m} \rightarrow \infty$
$\eta - \mu$	$\eta - \mu$ shadowed with $\underline{m} \rightarrow \infty$	$\eta - \mu$ shadowed with $\underline{m} \rightarrow \infty$
$\lambda - \mu$	$\lambda - \mu$ shadowed with $\underline{m} \rightarrow \infty$	$\lambda - \mu$ shadowed with $\underline{m} \rightarrow \infty$
One-sided Gaussian	One-sided Gaussian with $\underline{m} \rightarrow \infty$	One-sided Gaussian with $\underline{m} \rightarrow \infty$
Hoyt	Hoyt shadowed with $\underline{m} \rightarrow \infty$	Hoyt shadowed with $\underline{m} \rightarrow \infty$
Weibull	Weibull shadowed with $\underline{m} \rightarrow \infty$	Weibull shadowed with $\underline{m} \rightarrow \infty$
Negative exponential	Negative exponential shadowed with $\underline{m} \rightarrow \infty$	Negative exponential shadowed with $\underline{m} \rightarrow \infty$
Gamma	Gamma shadowed with $\underline{m} \rightarrow \infty$	Gamma shadowed with $\underline{m} \rightarrow \infty$
Nakagami- m	K_G with $\underline{m} \rightarrow \infty$	K_G with $\underline{m} \rightarrow \infty$
Rayleigh	K_G with $\underline{m} \rightarrow \infty$ and $m = 1$	K_G with $\underline{m} \rightarrow \infty$ and $m = 1$

with

$$a_i = \frac{\sqrt{(\eta_i - 1)^2 + 4\eta_i\lambda_i^2}}{1 - \lambda_i^2}, \quad \phi_i = \frac{\alpha_i}{2} \left(\mu_i + \frac{1}{2} \right),$$

$$\rho_i = \frac{\mu_i(1 + \eta_i)^2}{2\eta_i(1 - \lambda_i^2)\bar{\gamma}_i^{\alpha_i/2}}, \quad \vartheta_i = \frac{a_i\mu_i(1 + \eta_i)}{2\eta_i\bar{\gamma}_i^{\alpha_i/2}}.$$

The fading parameters are defined as follows. α_i stands for the non-linearity parameter, λ_i denotes the correlation

coefficient between the quadrature components and in-phase scattered waves, η_i indicates the ratio between the power of the quadrature and in-phase scattered components, and μ_i represents the real extension of the multipath clusters.

The PDF of Nakagami- m distribution is expressed as

$$f_{x_i}(x) = \frac{m_i^{m_i}}{\Gamma(m_i)} x^{m_i-1} e^{-m_i x}, \tag{20}$$

where m_i refers to the shadowing severity index.

According to [[19], equation (4)], the PDF of the product of two RVs can be evaluated by

$$f_{\gamma_i}(\gamma) = \int_0^\infty \frac{1}{r} f_{\gamma_i}\left(\frac{\gamma}{r}\right) f_{x_i}(r) dr. \quad (21)$$

Substituting (19) and (20) into (21), this obtains

$$f_{\gamma_i}(\gamma) = \frac{\psi_i m_i^{m_i}}{\Gamma(m_i)} \gamma^{\phi_i-1} \times \int_0^\infty r^{m_i-\phi_i-1} e^{-\rho_i \frac{\gamma^{\alpha_i/2}}{r^{\alpha_i/2}} - m_i r} I_{\mu_i-\frac{1}{2}}\left(\frac{\vartheta_i \gamma^{\alpha_i/2}}{r^{\alpha_i/2}}\right) dr. \quad (22)$$

Using the substitution $z = \rho_i \frac{\gamma^{\alpha_i/2}}{r^{\alpha_i/2}}$ into (22), this yields

$$f_{\gamma_i}(\gamma) = \frac{2\psi_i m_i^{m_i}}{\alpha_i \Gamma(m_i)} \rho_i^{\frac{2(m_i-\phi_i)}{\alpha_i}} \gamma^{\phi_i-1} \int_0^\infty e^{-z} g(z) dz, \quad (23)$$

$$\text{where } g(z) = z^{1-\frac{2(m_i-\phi_i)}{\alpha_i}} e^{-\frac{\rho_i}{z^{\frac{2}{\alpha_i}}} \gamma} I_{\mu_i-\frac{1}{2}}\left(\frac{\vartheta_i}{\rho_i} z\right).$$

With the help of a Gaussian–Laguerre quadrature approximation, the integration in (23), $\Lambda = \int_0^\infty e^{-z} g(z) dz$, can be expressed as $\Lambda \approx \sum_{l_i=0}^{L_i} w_{l_i} g(z_{l_i})$, where w_{l_i} and z_{l_i} are, respectively, the weight factors and abscissas defined in [44]. Consequently, (23) can be rewritten using (1) with the following parameters

$$\beta_{l_i} = m_i, \quad \zeta_{l_i} = m_i \frac{\rho_i^{2/\alpha_i}}{z_{l_i}^{2/\alpha_i}}, \quad \sigma_{l_i} = \frac{\theta_{l_i}}{\sum_{j_i=1}^{L_i} \theta_{j_i} \Gamma(\beta_{j_i}) \zeta_{j_i}^{-\beta_{j_i}}}$$

$$\theta_{l_i} = \frac{2\psi_i m_i^{m_i}}{\alpha_i \Gamma(m_i)} w_{l_i} \rho_i^{\frac{2(m_i-\phi_i)}{\alpha_i}} z_{l_i}^{1-\frac{2(m_i-\phi_i)}{\alpha_i}} I_{\mu_i-\frac{1}{2}}\left(\frac{\vartheta_i}{\rho_i} z_{l_i}\right). \quad (24)$$

5 | APPLICATIONS OF THE PRODUCT OF I.N.D. MG RVs TO CASCADED FADING CHANNELS

5.1 | Outage probability

The OP is an important performance metric of the wireless communications systems operating over fading channels and its defined as the probability that the output SNR drops below a predefined threshold value γ_{th} [45]. Consequently, the OP, P_o , of the AF-relay system that is demonstrated in Figure 1, can be calculated by [[45], equation (1.4)]

$$P_o = F_Y(\gamma_{th}), \quad (25)$$

where $F_Y(\cdot)$ is the CDF of the product of i.n.d. MG variates that is given in (3).

5.2 | Average bit/symbol error probability

In this section, the ABEP and the ASEP for several modulation schemes over cascaded fading channels that are represented by a MG distribution, are derived in exact unified closed-form expressions.

5.2.1 | Non-Coherent BFSK and DBPSK

The ABEP of non-coherent binary frequency shift keying (NC-BFSK) and differential binary phase shift keying (DBPSK), \bar{P}_b , can be computed by [[45], equation (9.254)]

$$\bar{P}_b = \frac{\mathcal{M}_Y(g_1)}{2}, \quad (26)$$

where $g_1 = 0.5$ and $g_1 = 1$ for NC-BFSK and DBPSK, respectively, and $\mathcal{M}_Y(\cdot)$ is provided in (4).

5.2.2 | Coherent BFSK, BPSK, and BFSK with minimum correlation

The ABEP of coherent BFSK, BPSK, and BFSK with minimum correlation can be evaluated by [[45], equation (9.11)]

$$\bar{P}_b^C = \frac{1}{\pi} \int_0^{\frac{\pi}{2}} \mathcal{M}_Y\left(\frac{g_2}{\sin^2 \theta}\right) d\theta, \quad (27)$$

where $g_2 = 0.5$, $g_2 = 1$, and $g_2 = 0.715$ for coherent BFSK, BPSK, and BFSK with minimum correlation, respectively.

Proposition 1. *The ABEP of coherent BFSK, BPSK, and BFSK with minimum correlation, \bar{P}_b^C , over cascaded fading conditions is obtained as*

$$\bar{P}_b^C = \frac{1}{2\sqrt{\pi} g_2} \sum_{l_1=1}^{L_1} \cdots \sum_{l_N=1}^{L_N} \Phi_N \times G_{2,N+1}^{N,2} \left[\frac{\Xi_N}{g_2} \middle| \begin{matrix} 0, -0.5 \\ (\beta_{l_i} - 1)_{i=1:N}, -1 \end{matrix} \right]. \quad (28)$$

Proof. Plugging (4) in (27) and using the change of the variable $x = \sin^2 \theta$ with some mathematical manipulations, we have

$$\bar{P}_b^C = \frac{1}{\pi} \sum_{l_1=1}^{L_1} \cdots \sum_{l_N=1}^{L_N} \frac{\Phi_N}{2g_2} \times \int_0^1 \frac{\sqrt{x}}{\sqrt{1-x}} G_{1,N}^{N,1} \left[\frac{\Xi_N}{g_2} x \middle| \begin{matrix} 0 \\ (\beta_{l_i} - 1)_{i=1:N} \end{matrix} \right] dx. \quad (29)$$

With the aid of the definition of the Meijer's G -function [[41], equation (1.112)] and the Fubini's theorem that is applied to interchange the order of the linear and closed integrations, (29) becomes

$$\begin{aligned} \bar{P}_b^C &= \frac{1}{\pi} \sum_{l_1=1}^{L_1} \dots \sum_{l_N=1}^{L_N} \frac{\Phi_N}{2g_2} \frac{1}{2\pi i} \int_{\mathcal{L}} \int_0^1 \frac{x^{\frac{1}{2}-t}}{\sqrt{1-x}} dx \\ &\times \Gamma(1-t) \left(\prod_{i=1}^N \Gamma(\beta_i - 1 + t) \right) \left(\frac{\Xi_N}{g_2} \right)^{-t} dt. \end{aligned} \quad (30)$$

It can be noted that the inner integral of (30) can be computed as

$$\int_0^1 \frac{x^{\frac{1}{2}-t}}{\sqrt{1-x}} dx \stackrel{(a)}{=} B\left(\frac{1}{2}, \frac{3}{2} - t\right). \quad (31)$$

where $B(.,.)$ is the Beta function defined in [[42], equation (8.380.1)] and (a) follows [[42], equation (3.191.3)].

Recalling the property [[42], equation (8.384.1)] for (31) and inserting the result in (30) and employing [[41] equation (1.112)], (28) is yielded and this completes the proof. \square

5.2.3 | MPSK

The ASEP of MPSK can be calculated by [[45], equation (9.15)]

$$\bar{P}_s^{MPSK} = \frac{1}{\pi} \int_0^{\pi - \frac{\pi}{M}} \mathcal{M}_Y \left(\frac{g_{PSK}}{\sin^2 \theta} \right) d\theta. \quad (32)$$

where $g_{PSK} = \sin^2 \frac{\pi}{M}$ with $M = 4, 8, 16, \dots$

$$\begin{aligned} \bar{P}_s^{MPSK} &= \sum_{l_1=1}^{L_1} \dots \sum_{l_N=1}^{L_N} \frac{\Phi_N}{g_{PSK}} \left\{ \frac{1}{\sqrt{\pi}} G_{2,N+1}^{N,2} \left[\frac{\Xi_N}{g_{PSK}} \middle| (\beta_i - 0.5)_{i=1:N}, -1 \right] \right. \\ &\quad \left. - \frac{g_{PSK}^{\frac{3}{2}}}{2} G_{1,1:1,N;1,1,0}^{0,1:N,1;1,0} \left[\Xi_N, g_{PSK} \middle| \begin{matrix} -0.5 & 0 & ; 0.5 \\ -1.5 & (\beta_i - 1)_{i=1:N} & ; 0 \end{matrix} \right] \right\}. \end{aligned} \quad (33)$$

Proposition 2. The ASEP of MPSK over cascaded fading channels using a MG distribution is given in (33) shown at the top of this page. In (33), $G_{\epsilon, d: \epsilon_1, d_1; \epsilon_2, d_2}^{a, b: a_1, b_1; a_2, b_2} [.]$ is the bivariate Meijer's G -function defined in [[46], equation (10)].

Proof. After performing simple mathematical manipulations, (32) can be rewritten as

$$\begin{aligned} \bar{P}_s^{MPSK} &= \overbrace{\frac{2}{\pi} \int_0^{\frac{\pi}{2}} \mathcal{M}_Y \left(\frac{g_{PSK}}{\sin^2 \theta} \right) d\theta}^{I_1} \\ &\quad - \underbrace{\frac{1}{\pi} \int_0^{\frac{\pi}{M}} \mathcal{M}_Y \left(\frac{g_{PSK}}{\sin^2 \theta} \right) d\theta}_{I_2}. \end{aligned} \quad (34)$$

One can see that I_1 can be evaluated by following the same methodology of the Proposition 1 as provided in the first term of (33).

For I_2 , we substitute (4) in (34) and assume $x = \sin^2 \theta$, to obtain

$$\begin{aligned} I_2 &= \frac{1}{2\sqrt{\pi} g_{PSK}} \sum_{l_1=1}^{L_1} \dots \sum_{l_N=1}^{L_N} \Phi_N \\ &\times \int_0^{g_{PSK}} \frac{\sqrt{x}}{\sqrt{1-x}} G_{1,N}^{N,1} \left[\frac{\Xi_N}{g_{PSK}} x \middle| \begin{matrix} 0 \\ (\beta_i - 1)_{i=1:N} \end{matrix} \right] dx. \end{aligned} \quad (35)$$

Using the definition of the Meijer's G -function [[41], equation (1.112)] and the Fubini's theorem, the following integral is deduced

$$\begin{aligned} I_2 &= \frac{1}{2\sqrt{\pi} g_{PSK}} \sum_{l_1=1}^{L_1} \dots \sum_{l_N=1}^{L_N} \Phi_N \\ &\times \frac{1}{2\pi i} \int_{\mathcal{L}} \int_0^{g_{PSK}} \frac{x^{\frac{1}{2}-t}}{\sqrt{1-x}} dx \Gamma(1-t) \\ &\quad \left(\prod_{i=1}^N \Gamma(\beta_i - 1 + t) \right) \left(\frac{\Xi_N}{g_{PSK}} \right)^{-t} dt. \end{aligned} \quad (36)$$

The inner integral of (36) can be expressed as

$$\begin{aligned} \int_0^{g_{PSK}} \frac{x^{\frac{1}{2}-t}}{\sqrt{1-x}} dx &\stackrel{(b_1)}{=} \frac{g_{PSK}^{\frac{3}{2}-t}}{\frac{3}{2}-t} {}_2F_1 \left(\frac{3}{2} - t, \frac{1}{2}; \frac{5}{2} - t; g_{PSK} \right) \\ &\stackrel{(b_2)}{=} \sqrt{\pi} g_{PSK}^{\frac{3}{2}-t} G_{3,3}^{1,2} \left[g_{PSK} \middle| \begin{matrix} t - 0.5, 0.5, 0.5 \\ 0, t - 1.5, 0.5 \end{matrix} \right], \end{aligned} \quad (37)$$

where ${}_2F_1(.,.,.;.)$ is the hypergeometric function defined in [[42], equation (9.14.1)]. Step (b₁) follows [[42], equation (8.391)] whereas (b₂) is obtained after using the identities [[42], equation (8.331.1)] and [[47], equation (07.23.26.0005.01)] with some mathematical simplifications.

Recalling [[41], equation (1.112)] for the Meijer's G -function of (37) and substituting the result into (36) to yield

$$\begin{aligned} I_2 &= \frac{\sqrt{g_{PSK}}}{2} \sum_{l_1=1}^{L_1} \dots \sum_{l_N=1}^{L_N} \Phi_N \\ &\frac{1}{(2\pi i)^2} \int_{\mathcal{L}} \int_{\mathcal{T}} \frac{\Gamma(1.5-t-r) \left(\prod_{i=1}^N \Gamma(\beta_i - 1 + t) \right) \Gamma(1-t) \Gamma(r)}{\Gamma(2.5-t-r) \Gamma(0.5+r)} \\ &\quad \Xi_N^{-t} g_{PSK}^{-r} dt dr. \end{aligned} \quad (38)$$

With the aid of [[46], equation (10)], \mathcal{I}_2 can be written in exact closed-form as shown in the second term of (33) which completes the proof. \square

5.2.4 | MQAM

The ASEP of MQAM can be computed by [[45], equation (9.21)]

$$\bar{P}_s^{MQAM} = 4c(\mathcal{J}_1 - c\mathcal{J}_2), \quad (39)$$

where $c = 1 - \frac{1}{\sqrt{M}}$,

$$\mathcal{J}_1 = \frac{1}{\pi} \int_0^{\frac{\pi}{2}} \mathcal{M}_Y \left(\frac{g_{QAM}}{\sin^2 \theta} \right) d\theta, \quad (40)$$

and

$$\mathcal{J}_2 = \frac{1}{\pi} \int_0^{\frac{\pi}{4}} \mathcal{M}_Y \left(\frac{g_{QAM}}{\sin^2 \theta} \right) d\theta, \quad (41)$$

with $g_{QAM} = \frac{3}{2(M-1)}$ where $M = 4, 8, 16, \dots$

$$\begin{aligned} \bar{P}_s^{MQAM} = & \sum_{l_1=1}^{L_1} \dots \sum_{l_N=1}^{L_N} \frac{2c\Phi_N}{g_{QAM}} \left\{ \frac{1}{\sqrt{\pi}} G_{2,N+1} \left[\frac{\Xi_N}{g_{QAM}} \middle| \begin{matrix} 0, -0.5 \\ (\beta_{l_i} - 1)_{i=1:N}, -1 \end{matrix} \right] \right. \\ & \left. - \frac{c}{\sqrt{8}} G_{1,1:N,1,1,0} \left[\frac{\Xi_N}{2g_{QAM}}, 0.5 \middle| \begin{matrix} -0.5: & 0 & ; 0.5 \\ -1.5: (\beta_{l_i} - 1)_{i=1:N}; 0 \end{matrix} \right] \right\}. \end{aligned} \quad (42)$$

It can be noted that \mathcal{J}_1 can be calculated by using the same steps of deriving \bar{P}_b^C in (28), namely, Proposition 1 as shown in the first term of (42) given at the top of this page. In addition, \mathcal{J}_2 can be derived by following the same procedure that is employed to derive \mathcal{I}_2 of (34) after inserting $M = 4$. Consequently, \bar{P}_s^{MQAM} is obtained in exact closed-form expression as shown in (42) given at the top of this page.

5.3 | Effective rate of wireless communications systems

The ER has been proposed to measure the performance of the wireless communications systems under the quality of service (QoS) constraints, such as system delays, that have been neglected by Shannon theorem [48]. Hence, this performance metric has been widely analysed over differ-

ent fading channels in the open technical literature (see [33] and [49] and references therein). However, there is no work has been achieved to study the ER over cascaded fading channels which is one of our contributions in this paper.

The ER, R , can be calculated by [[33], equation (1)]

$$R = -\frac{1}{\mathcal{A}} \log_2 \left(\mathbb{E}\{(1+y)^{-\mathcal{A}}\} \right), \quad (43)$$

where $\mathcal{A} \triangleq \theta TB / \ln 2$ with θ , T , and B are, respectively, the delay exponent, block duration, and bandwidth of the system and $\mathbb{E}\{\cdot\}$ stands for the expectation.

It can be noticed that (43) can be written as [[49], equation (8)]

$$R = -\frac{1}{\mathcal{A}} \log_2 \left(\int_0^\infty (1+y)^{-\mathcal{A}} f_Y(y) dy \right). \quad (44)$$

Now, the ER over unified cascaded fading channels using a MG distribution can be derived after inserting (2) in (44) and utilising [[41], equation (1.112)] and the Fubini's theorem. Thus, this yields

$$\begin{aligned} R = & -\frac{1}{\mathcal{A}} \log_2 \left(\sum_{l_1=1}^{L_1} \dots \sum_{l_N=1}^{L_N} \Phi_N \frac{1}{2\pi i} \int_{\mathcal{L}} \prod_{i=1}^N \Gamma(\beta_{l_i} - 1 + t) \right. \\ & \left. \times (\Xi_N)^{-t} \int_0^\infty (1+y)^{-\mathcal{A}} y^{-t} dy dt \right). \end{aligned} \quad (45)$$

Invoking [[42], equation (3.194.3)] to compute the inner integral of (45) and making use of the identity [[42], equation (8.384.1)] and [[41], equation (1.112)], the following closed-form expression is deduced

$$\begin{aligned} R = & -\frac{1}{\mathcal{A}} \log_2 \left(\sum_{l_1=1}^{L_1} \dots \sum_{l_N=1}^{L_N} \frac{\Phi_N}{\Gamma(\mathcal{A})} \right. \\ & \left. G_{1,N+1}^{N+1,1} \left[\Xi_N \middle| \begin{matrix} 0 \\ (\beta_{l_i} - 1)_{i=1:N}, \mathcal{A} - 1 \end{matrix} \right] \right). \end{aligned} \quad (46)$$

5.4 | AUC of energy detection-based spectrum sensing

The ED technique has been widely employed to perform the spectrum sensing in both cognitive radio (CR) and ultra-wide band (UWB) systems. This refers to its low implementation intricacy where the unlicensed user, namely, secondary user (SU), does not need a prior information about the licensed user

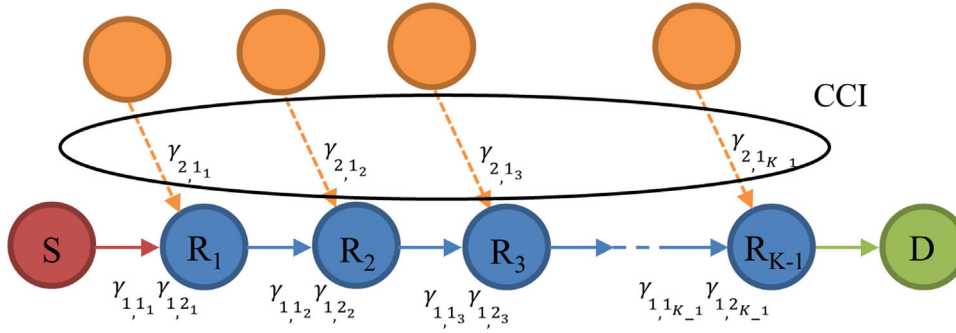


FIGURE 3 Multi-hop communication system by DF-relay nodes with CCI [6]

(PU) [30], [31], [49, 50] as demonstrated in Figure 2. To study the behaviour of an ED, the receiver operating characteristics (ROC) curve which plots the ADP versus the false alarm probability is utilised in many efforts. But, in some cases, this performance metric does not provide a clear result on the superiority of one system on the other. This is due to the intersection between the two compared curves in specific values of ADP and false alarm probability. Based on this observation, the authors in [50] proposed the average AUC curve as another performance metric of an ED via measuring the total area under the ROC.

The average AUC, \bar{A} , can be evaluated by [[49], equation (21)]

$$\bar{A} = \int_0^{\infty} \mathcal{A}(y) f_Y(y) dy, \quad (47)$$

where $\mathcal{A}(y)$ is the AUC in additive white Gaussian noise (AWGN) environment which is expressed as [[49], equation (20)]

$$\mathcal{A}(y) = 1 - \sum_{r=0}^{u-1} \sum_{n=0}^r \binom{r+n-1}{r-n} \frac{y^n e^{-\frac{y}{2}}}{2^{r+n} n!}, \quad (48)$$

where $\binom{b}{a}$ denotes the binomial coefficient.

The average AUC over cascaded fading conditions can be obtained after plugging (2) and (48) in (47) and invoking the fact that $\int_0^{\infty} f_Y(y) dy \triangleq 1$ and [[41], equation (2.29)]. Accordingly, we have

$$\bar{A} = 1 - \sum_{r=0}^{u-1} \sum_{n=0}^r \binom{r+n-1}{r-n} \frac{1}{2^{r+n} n!} \sum_{l_1=1}^{L_1} \cdots \sum_{l_N=1}^{L_N} \Phi_N G_{1,N}^{N,1} \left[\frac{\Xi_N}{2} \middle| \begin{matrix} -n \\ (\beta_{l_i} - 1)_{i=1:N} \end{matrix} \right]. \quad (49)$$

To the best of the authors' knowledge, (49) is new and there is no work has been devoted to study the average AUC over cascaded fading channels.

6 | APPLICATIONS OF THE RATIO OF THE PRODUCTS OF I.N.D. MG RVs IN WIRELESS COMMUNICATION SYSTEMS

6.1 | Outage probability of multi-hop wireless communications system with CCI

In this section, the OP of the multi-hop wireless communications system with DF relaying and interferer at each hop is analysed. In this system that is shown in Figure 3, the number of hops is K and the signal-to-interference ratio at the input of r -th terminal with $r \in \{1, K-1\}$, is assumed to be $X_r = \frac{\gamma_{1,1,r} \gamma_{1,2,r}}{\gamma_{2,1,r}}$ where $\gamma_{1,1,r}$, $\gamma_{1,2,r}$, and $\gamma_{2,1,r}$ are the RVs that represent the impact of the fading, the shadowing, and the co-channel interference, respectively [6].

According to [[6], equation (23)], the OP of K -hop wireless communication systems, $P_o^{(K)}$, can be computed by

$$P_o^{(K)} = 1 - \prod_{r=1}^K (1 - F_{X_r}(\gamma_{th})), \quad (50)$$

where γ_{th} is the threshold value and $F_{X_r}(\cdot)$ is the CDF that is given in (11) with $N = 2$ and $M = 1$.

Based on (50), for dual-hop, that is, $K = 2$, the OP, $P_o^{(2)}$, is written as [[6], equation (24)]

$$P_o^{(2)} = F_{X_1}(\gamma_{th}) + F_{X_2}(\gamma_{th}) - F_{X_1}(\gamma_{th})F_{X_2}(\gamma_{th}). \quad (51)$$

Additionally, for $K = 3$, namely, triple-hop, the OP, $P_o^{(3)}$, is expressed as [[6], equation (25)]

$$\begin{aligned} P_o^{(3)} &= F_{X_1}(\gamma_{th}) + F_{X_2}(\gamma_{th}) + F_{X_3}(\gamma_{th}) \\ &\quad - F_{X_1}(\gamma_{th})F_{X_2}(\gamma_{th}) - F_{X_1}(\gamma_{th})F_{X_3}(\gamma_{th}) \\ &\quad - F_{X_2}(\gamma_{th})F_{X_3}(\gamma_{th}) + F_{X_1}(\gamma_{th})F_{X_2}(\gamma_{th})F_{X_3}(\gamma_{th}). \end{aligned} \quad (52)$$

6.2 | Physical layer security

The performance of the PLS over different fading channel models has been given a special consideration by many works in the

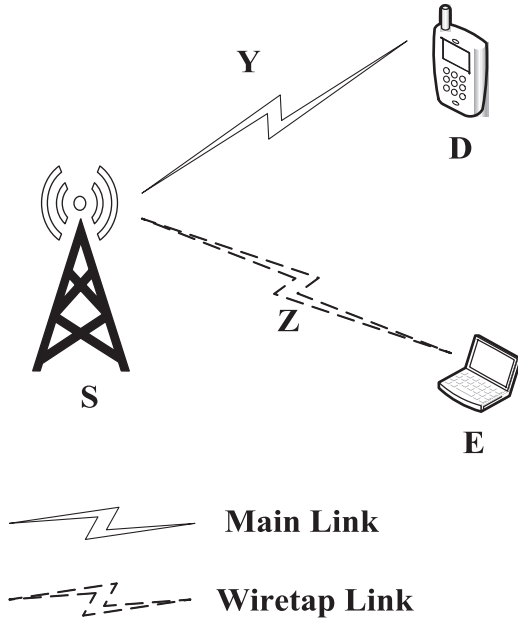


FIGURE 4 A wireless network consisting of a transmitter **S** (Alice) and a legitimate receiver **D** (Bob) in the presence of an eavesdropping attack **E** (Eve) [51]

literature. This is because it is able to fortify the security of the wireless link [22].

In this work, we have assumed the transmitter (**S**) communicates with the legitimate receiver (**D**) via the main channel in the presence of an eavesdropper (**E**), as illustrated in Figure 4. Therefore, the channel state information (CSI) of **D** can be known by **S** whereas a perfect knowledge of the CSI of **E** cannot be assumed at **S** and hence information-theoretic security cannot be guaranteed. Moreover, both the main and wiretap channels are supposed to be independent and undergo quasi-static fading channels that are modelled by using a MG distribution. Also, we have assumed all **S**, **D** and **E** are equipped with a single received antenna [51].

6.2.1 | Lower bound of secure outage probability

One of the main performance measurements of the PLS is the secure outage probability (SOP) [22], [34], [35], [40]. However, its difficult to derive the SOP in a unified exact closed-form computationally tractable expression [40], [51]. Therefore, the lower bound of the SOP (SOP^L) is utilised in many studies in the analysis of the PLS.

The SOP^L can be evaluated by [[7], equation (39)]

$$\text{SOP}^L = F_X(\epsilon), \quad (53)$$

where $X = \frac{\gamma_D}{\gamma_E}$ is defined in Theorem 2, γ_D and γ_E are the received SNR at **D** and **E**, respectively, $F_X(\cdot)$ is given in (11), and $\epsilon = 2^{R_{th}}$ with R_{th} denotes the target secrecy rate threshold.

In contrast to the SOP^L of [[35], equation (6)] that is given for a single path and [[38], equation (27)] that is included an infinite series, (53) is derived in a simple unified closed-form expression and it can be applied for a wide range of the cascaded fading conditions.

6.2.2 | Probability of non-zero secrecy capacity

Another metric that is used to analyse the performance of the PLS is the PNSC which means the secrecy capacity is always positive.

The PNSC can be readily obtained from (53) as follows

$$\text{PNSC} = 1 - F_X(1). \quad (54)$$

6.3 | Spectrum sharing in cognitive radio networks

As its explained in Section 5.4, in the CRNs, the SU can employ the spectrum of the PU when the interference between the transmitted signal by the SU transmitter (**SU-Tx**) and the PU receiver (**PU-Rx**). In this figure, the power gain of the instantaneous channel from the **SU-Tx** to the PU receiver (**PU-Rx**) and from the **SU-Tx** to the SU receiver (**SU-Rx**) are represented by **Z** and **Y**, respectively.

In this work, **Z** and **Y** are assumed to be independent with channel coefficients following a MG distribution and subjected to AWGN with zero mean and variance N_0 which stands for the single-sided AWGN.

6.3.1 | Outage capacity

The outage capacity (OC), C_o , is used to quantify the spectral efficiency over fading channels. It can be defined as the probability of the instantaneous capacity is less than a certain value of the transmission rate R_0 . Accordingly, for the spectrum sharing network that is shown in Figure 2, $C_o = Pr\left\{\frac{Y}{Z} < \frac{N_0(2^{R_0}-1)}{Q_{pk}}\right\}$ where Pr stands for the probability and Q_{pk} is the peak received power limits at the **PU-Rx** side [9].

Mathematically, C_o can be computed by [[9], equation (59)]

$$C_o = F_X\left(\frac{N_0(2^{R_0}-1)}{Q_{pk}}\right), \quad (55)$$

where $F_X(\cdot)$ is provided in (11) with $N = 1$ and $M = 1$, that is, $X = \frac{Y}{Z} = \frac{\gamma_{1,1}}{\gamma_{2,1}}$.

6.3.2 | Delay-limited capacity

The delay-limited capacity, C_d , can be defined as the maximum value of R_0 that is achievable over each of the fading blocks and

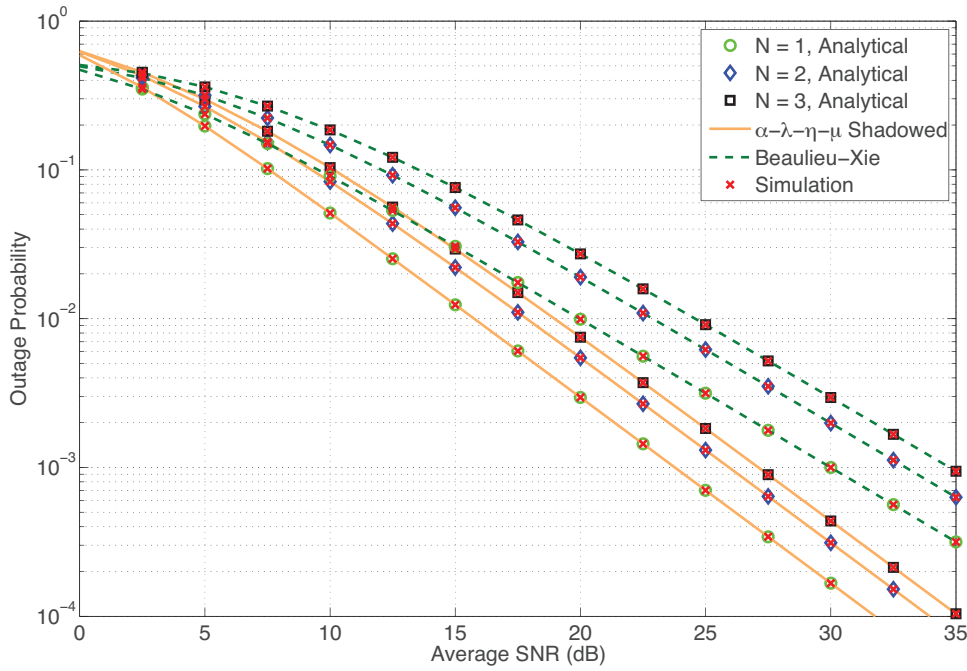


FIGURE 5 OP of cascaded Beaulieu–Xie and $\alpha - \lambda - \eta - \mu$ shadowed fading channels with $\gamma_{th} = 0$ dB

it can be calculated by [[9], equation (63)]

$$C_d = \log_2 \left[1 + \frac{Q_{avg}}{N_0 \mathbb{E}[X]} \right], \quad (56)$$

where Q_{avg} is the average interference power at the **PU-Rx** and $\mathbb{E}[\cdot]$ is the expectation operator.

Substituting (10) into (56) with $N = 1$ and $M = 1$ and recalling [[41], equation (2.9)], C_d is yielded as

$$C_d = \log_2 \left[1 + \frac{Q_{avg}}{N_0 \sum_{r=1,2}^{L_r} \frac{\Phi_{\lambda_1} \Phi_{\lambda_2} \Xi_{\lambda_1}}{\Xi_{\lambda_2}} \Gamma(\beta_{\lambda_1} - 1) \Gamma(\beta_{\lambda_2} + 1)} \right]. \quad (57)$$

7 | ANALYTICAL AND SIMULATION RESULTS

In this section, the numerical results of our derived expressions are compared with their Monte Carlo simulations that are obtained via running 10^6 iterations. In all figures, the minimum number of terms for i^{th} path, L_i , that satisfies $\text{MSE} \leq 10^{-5}$ is chosen to be 15. Additionally, all paths are assumed to be independent but not necessarily identically distributed. For further validations, in some figures, the results for the Rayleigh fading which is a special case of both the $\alpha - \lambda - \eta - \mu$ shadowed and the Fisher–Snedecor \mathcal{F} fading [9] via inserting $m_s \rightarrow \infty$ and $m = 1$ are compared.

Figure 5 shows the OP of cascaded Beaulieu–Xie and $\alpha - \lambda - \eta - \mu$ shadowed (format 1) fading channels with $\gamma_{th} = 0$ dB for three paths, namely, $N = 1, 2,$ and 3 , with $(m_1, m_2, m_3) = (1, 2, 3)$ for both fading channels¹. In this figure, $\lambda_1 = \lambda_2 = \lambda_3 = 0.5$ for Beaulieu–Xie fading model, whereas $\alpha_1 = \alpha_2 = \alpha_3 = 2.5, \lambda_1 = \lambda_2 = \lambda_3 = 0.1, \eta_1 = \eta_2 = \eta_3 = 0.5$, and $\mu_1 = \mu_2 = \mu_3 = 2.5$ for $\alpha - \lambda - \eta - \mu$ shadowed fading channel. For the same simulation parameters of Figure 5, Figures 6 and 7 compare between the ABEP of BPSK with the ASEP of 4PSK and 8QAM modulation schemes over Beaulieu–Xie and $\alpha - \lambda - \eta - \mu$ shadowed cascaded fading channels, respectively. Figures 8 and 9 illustrate the ER with $\mathcal{A} = 2.5$ and the average complementary AUC which is $1 - \bar{\mathcal{A}}$ for $u = 3$ versus the average SNR, respectively, and for the same fading parameters of Figure 1. As anticipated, the performance of the system decreases when the number of paths increases. This refers to the increase in the impact of the channel parameters on the transmitted signal which becomes high when N is large. For instance, in Figure 5, at fixed $\bar{\gamma} = 15$ dB, the values of the OP of cascaded Beaulieu–Xie and $\alpha - \lambda - \eta - \mu$ shadowed fading channels are reduced by approximately 44.89% and 43.84%, respectively, when N changes from 2 to 1. In the same context, at $N = 3$, the OP of Beaulieu–Xie fading condition is nearly 0.076 whereas for $\alpha - \lambda - \eta - \mu$ shadowed fading channels is roughly 0.029. One can see that the results of Figure 5 have been affirmed by Figures 6 and 7 via carrying out a comparison between the ABEP of BPSK with the ASEP of 4PSK and 8QAM modulation techniques. Moreover, Figure 8

¹ The results for format 2 can be easily deduced from format 1 via applying the bilinear transform where $\eta_{format2} = \frac{1 - \eta_{format1}}{1 + \eta_{format1}}$.

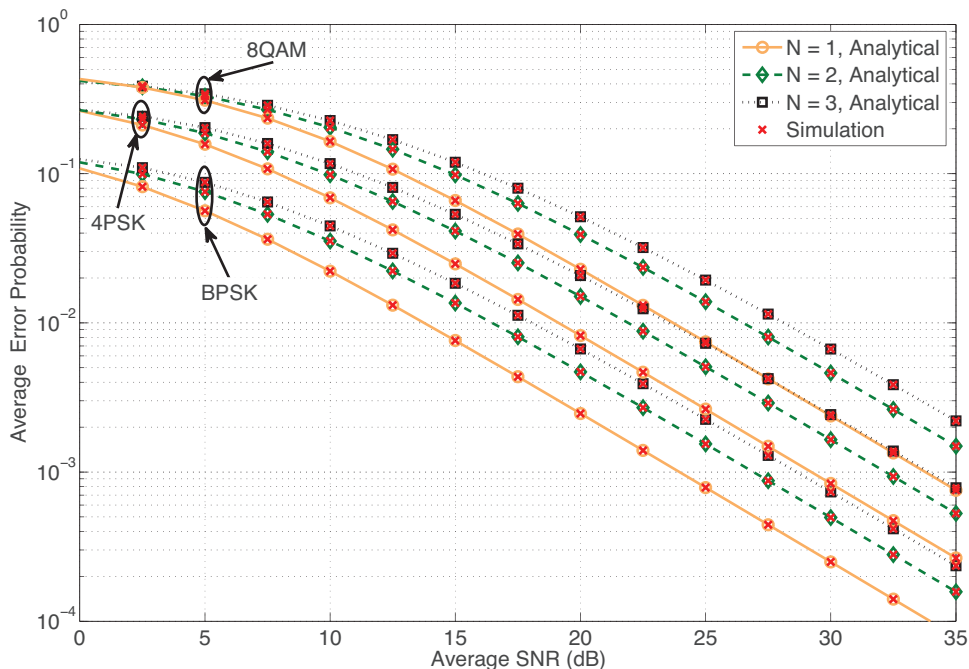


FIGURE 6 ABEP of BPSK and ASEP of 4PSK and 8QAM modulation schemes over cascaded Beaulieu–Xie fading channels

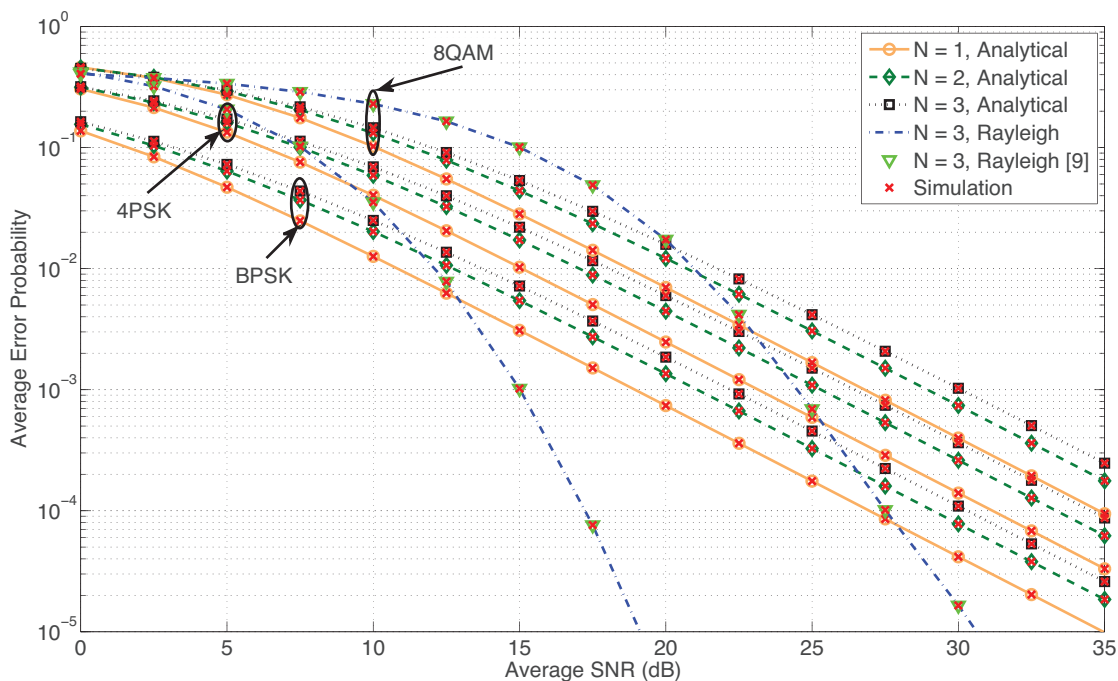


FIGURE 7 ABEP of BPSK and ASEP of 4PSK and 8QAM modulation schemes over cascaded $\alpha - \lambda - \eta - \mu$ shadowed fading channels

explains how the cascaded fading channels affects on the QoS of wireless communication systems via diminishing the ER. Additionally, in Figure 9, the average complementary AUC becomes low when the number of paths decreases. This is due to the increasing in both the missed-ADP and false alarm probability.

Figure 10 demonstrates the OP of DF relaying based multi-hop wireless communications systems with multiple interferers for $\gamma_{th} = 0$ dB. The analysis in this figure is provided for three types of i.n.d. hops which are $K = 1$ that represents a direct link, $K = 2$, and $K = 3$ via using the same fading parameters m for both channels, and λ, α , and η of $\alpha - \lambda - \eta - \mu$

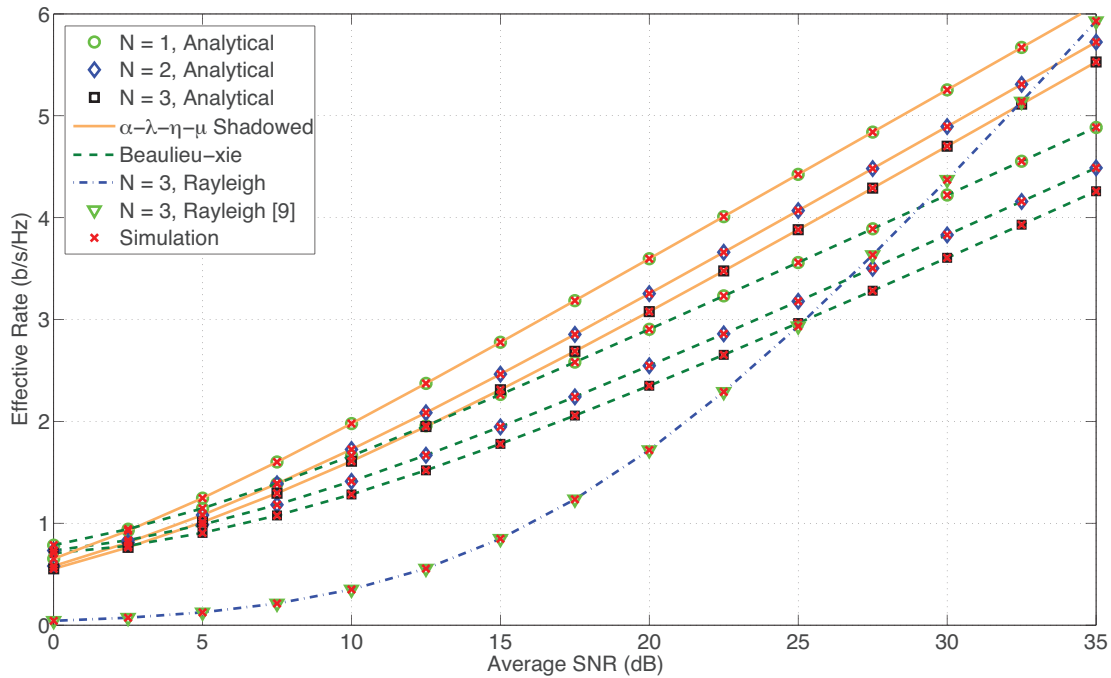


FIGURE 8 ER of cascaded Beaulieu-Xie and $\alpha - \lambda - \eta - \mu$ shadowed fading channels with $\mathcal{A} = 2.5$

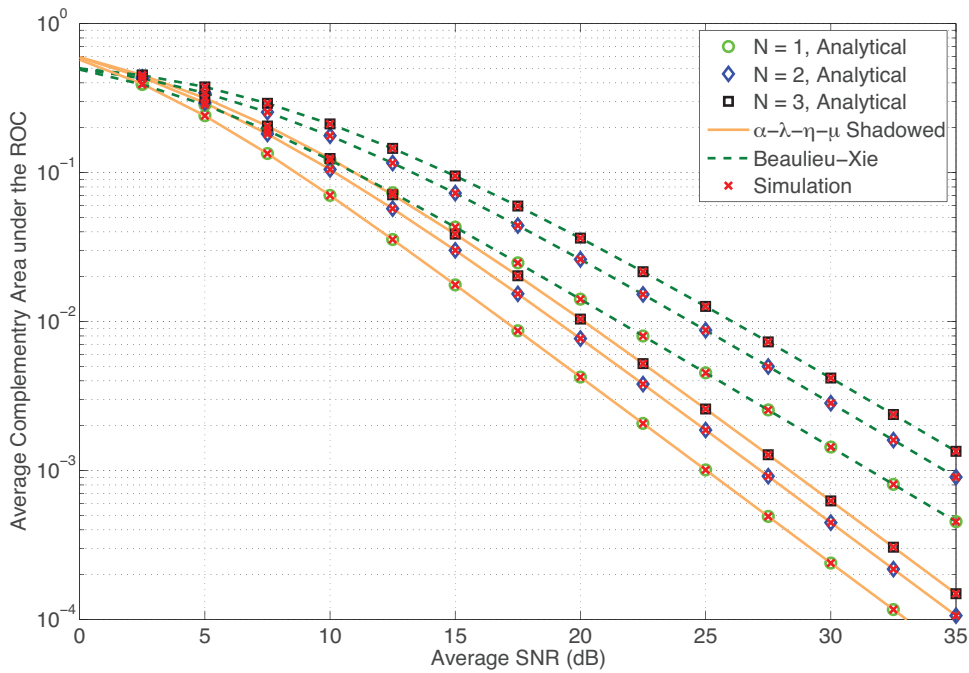


FIGURE 9 Average complementary AUC of cascaded Beaulieu-Xie and $\alpha - \lambda - \eta - \mu$ shadowed fading channels with $\nu = 3$

shadowed fading of Figure 5 and for all hops. However, for Beaulieu-Xie fading channels, $\lambda_1 = \lambda_2 = \lambda_3 = 0.5$ in the first hop, $\lambda_1 = \lambda_2 = \lambda_3 = 1.5$ in the second hop, and $\lambda_1 = \lambda_2 = \lambda_3 = 2.5$ in the third hop. In addition, for $\alpha - \lambda - \eta - \mu$ shadowed fading, $\mu_1 = \mu_2 = \mu_3 = 2.5$, $\mu_1 = \mu_2 = \mu_3 = 1.5$, and $\mu_1 = \mu_2 = \mu_3 = 0.5$ for the first, second, and third hops,

respectively. Similar to Figure 5, the OP drops when the number of hops, K , reduces. This observation is matched with the results that were presented in [6].

Figures 11 and 12 plot the SOP^{L_s} for $R_{th} = 1$ and PNSC, respectively, versus $\Psi = \frac{\tilde{\gamma}_D}{\tilde{\gamma}_E}$ and for different values of $\tilde{\gamma}_E$. For both fading channels, $m = 1$ for **D** and $m = 2$ for **E**. Besides,

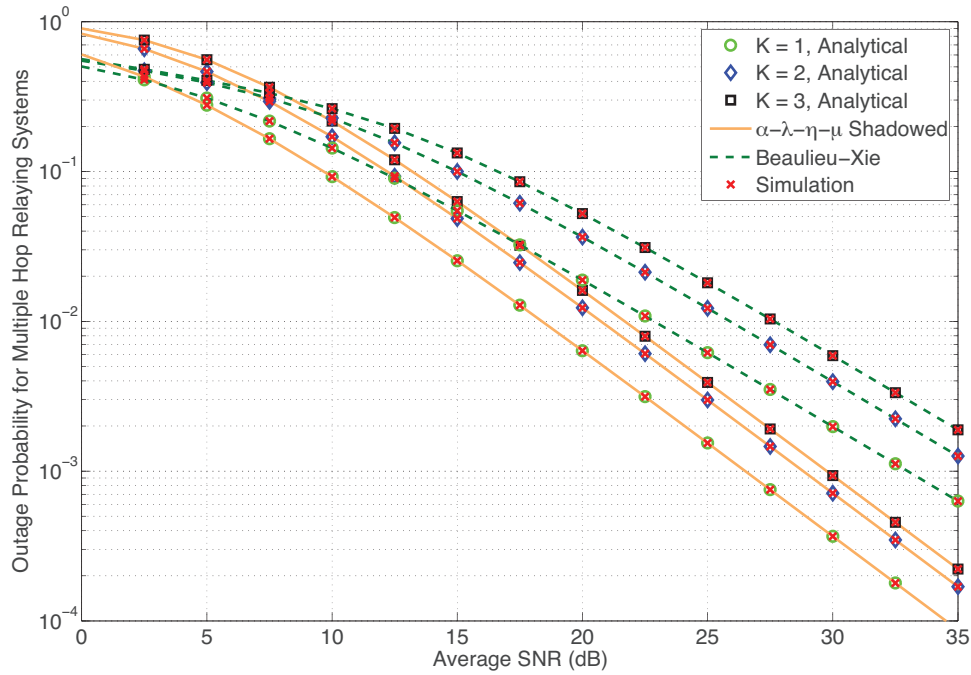


FIGURE 10 OP of DF relaying communication systems over Beaulieu–Xie and $\alpha - \lambda - \eta - \mu$ shadowed fading channels with $\gamma_{th} = 0$ dB

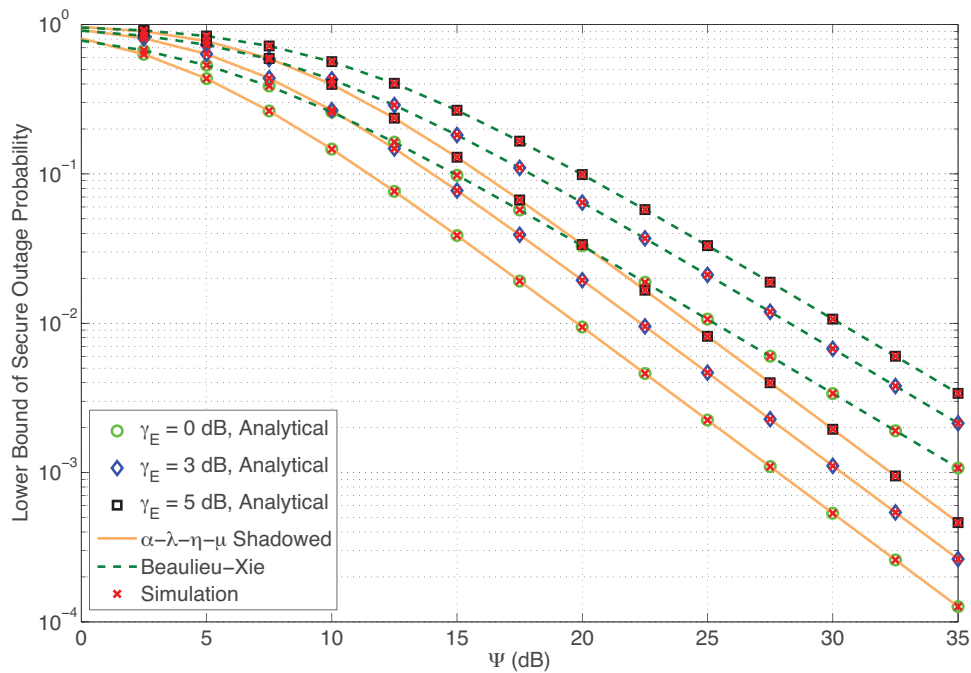


FIGURE 11 SOP^L versus Ψ over Beaulieu–Xie and $\alpha - \lambda - \eta - \mu$ shadowed fading channels with $R_{th} = 1$

in the Beaulieu–Xie fading channels, $\lambda = 0.5$ for both \mathbf{D} and \mathbf{E} whereas for $\alpha - \lambda - \eta - \mu$ shadowed fading, the parameters for both \mathbf{D} and \mathbf{E} are equal where $\alpha = 2.5$, $\lambda = 0.1$, $\eta = 0.5$, and $\mu = 2.5$. From both figures, a substantial degradation in the secrecy performance of the system can be noticed when the value of $\bar{\gamma}_E$ rises. This is because the large improvement

in the wiretap channel, namely, $\mathbf{S-E}$ link in comparison with the main channel. For example, in Figure 11 and at constant $\Psi = 10$ dB, the values of the SOP^L for $\bar{\gamma}_E = 3$ dB are higher than that of $\bar{\gamma}_E = 0$ dB by nearly 65.6% and 82.1% for Beaulieu–Xie and $\alpha - \lambda - \eta - \mu$ shadowed fading channels, respectively. This situation is consistent with the results that

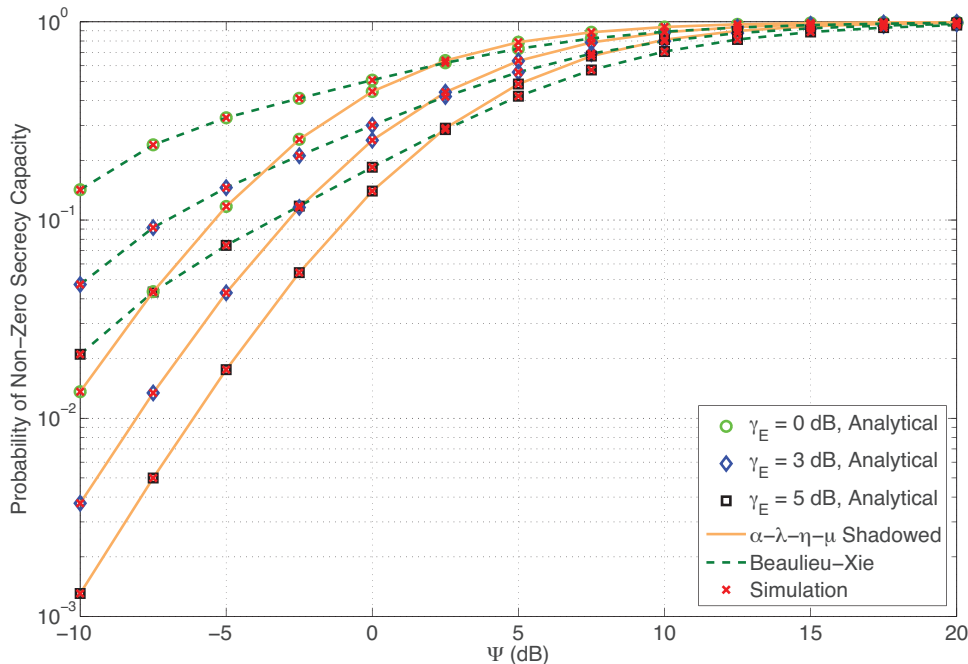


FIGURE 12 PNSC versus Ψ over Beaulieu–Xie and $\alpha - \lambda - \eta - \mu$ shadowed fading channels

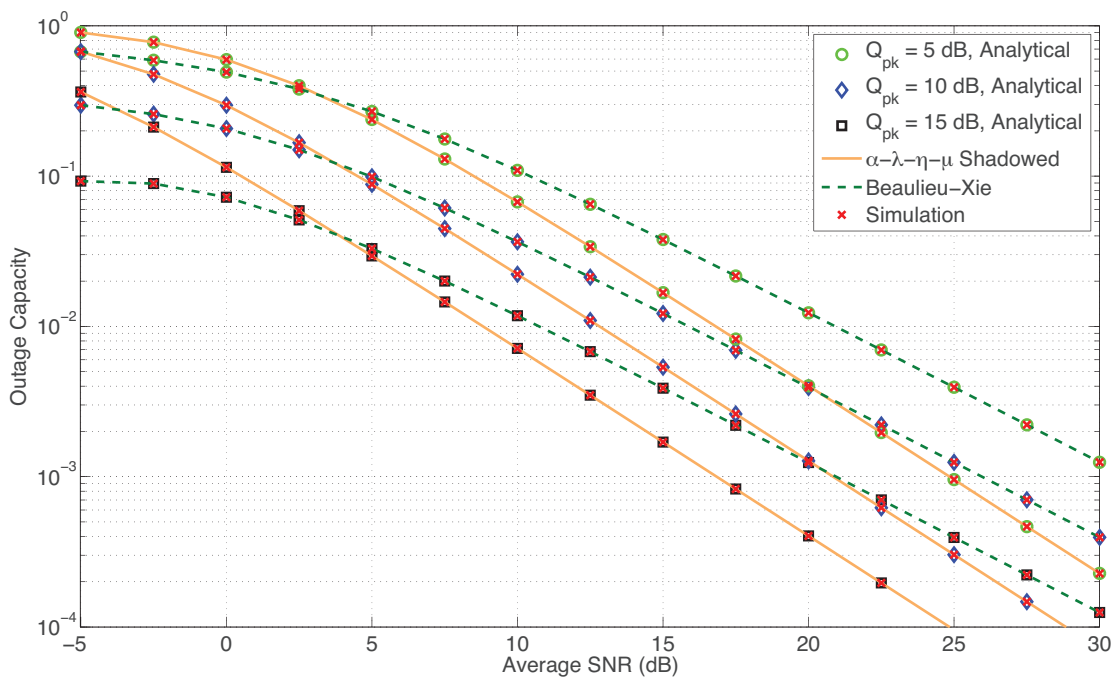


FIGURE 13 OC of CRNs over Beaulieu–Xie and $\alpha - \lambda - \eta - \mu$ shadowed fading channels with $R_0 = 1$ bits/Hz and $N_0 = 1$ W/Hz

were obtained in [34], [35] and [40] but for the K_C fading conditions.

Figure 13 depicts the OC of the CRNs versus the average SNR for $Q_{pk} = 5, 10,$ and 15 dB, $R_0 = 1$ bits/Hz, $N_0 = 1$ W/Hz and the same fading parameters of Figure 11. The figure explains that the OC decreases when Q_{pk} increases. This is because the increase in Q_{pk} gives more flexibil-

ity to the **SU-Tx** in transmitting the signals with higher power.

Figure 14 portrays the delay-limited capacity, C_d , versus the average SNR for $Q_{avg} = 5, 10,$ and 15 dB with $N_0 = 1$ W/Hz. It can be observed that as Q_{avg} increases, C_d improves.

In all presented figures, one can observe that the numerical results are perfectly coincided with their simulation

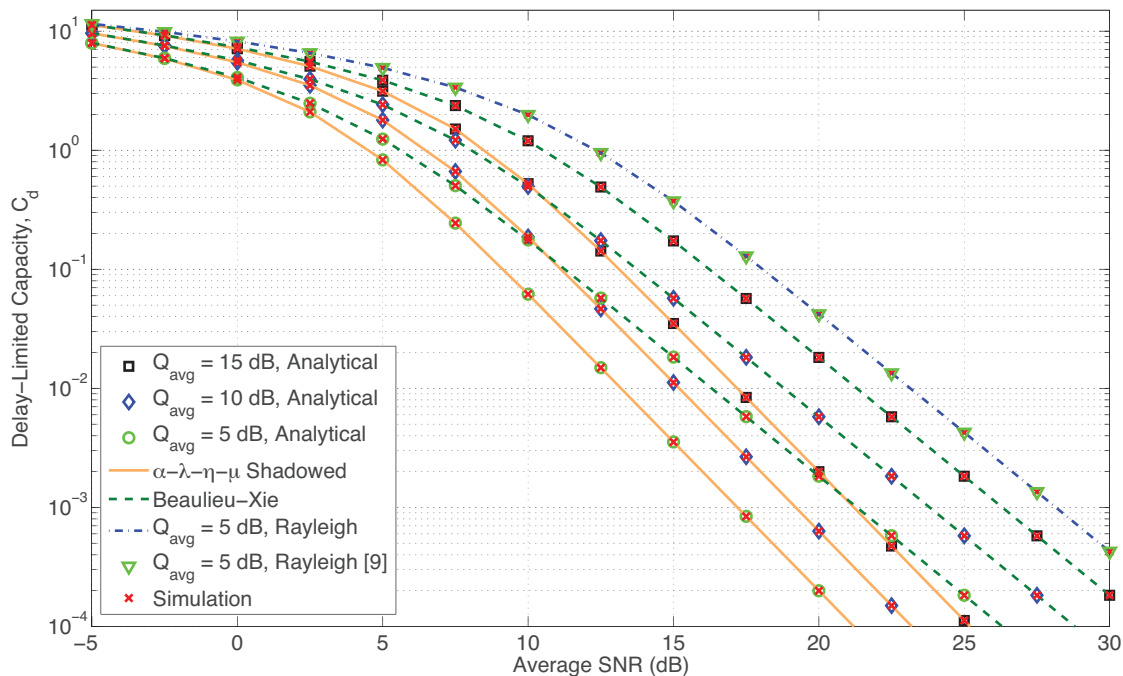


FIGURE 14 Delay-limited capacity of CRNs over Beaulieu–Xie and $\alpha - \lambda - \eta - \mu$ shadowed fading channels with $N_0 = 1$ W/Hz

counterparts which confirms the correctness of our derived expressions. Moreover, the results of our work for the Rayleigh fading that are plotted in Figures 7, 8 and 14 are in excellent matching with the analysis of [9] which proves the validation of our provided statistical properties.

8 | CONCLUSIONS

In this paper, the statistical characterisations of the product of i.n.d. MG variates were derived first. Thereafter, the study was extended to include the PDF, CDF, and MGF of the ratio of products of arbitrary distributed MG RVs. Based on these statistics, several performance metrics of wireless communication systems were analysed over cascaded Beaulieu–Xie and $\alpha - \lambda - \eta - \mu$ shadowed fading channels. In particular, the OP, ABEP, ASEP, ER, and average AUC of energy detection were provided in simple unified closed-form computationally tractable expressions. Furthermore, the OP of DF relaying of multi-hop wireless communication systems with CCI and the performance metrics of the PLS, namely, the SOP^L and PNSC were given. The numerical results for different number of paths and hops as well as the average SNR of the eavesdropper were presented. The outage and delay-limited capacities of the spectrum sharing in CRNs were also studied. These results showed how the performance of the systems diminishes when the aforementioned parameters are increased. Moreover, a comparison between the results of some performance metrics over Rayleigh fading channel which is a special case of $\alpha - \lambda - \eta - \mu$ shadowed fading and previous work, namely, [9] was carried out. The derived expressions of this work can be employed for all the

fading channels of Table 2 that can be represented by an MG distribution. Additionally, the generalisation of Beaulieu–Xie and $\alpha - \lambda - \eta - \mu$ shadowed fading conditions can be exploited to study the behaviour of the wireless communication systems over a variety of fading scenarios that are special cases of these channels, for example, $\alpha - \lambda - \eta - \mu$ by plugging $m \rightarrow \infty$.

ORCID

Hussien Al-Hmood  <https://orcid.org/0000-0001-7637-5624>

REFERENCES

1. Karagiannidis, G.K., et al.: Bounds for multihop relayed communications in Nakagami- m fading. *IEEE Trans. Commun.* 54(1), 18–22 (2006)
2. Ghobaei-Arani, M., Souri, A.: LP-WSC: a linear programming approach for web service composition in geographically distributed cloud environments. *J. Supercomput* 75, 2603–2628 (2019)
3. Peppas, K., et al.: Cascaded generalised- K fading channel. *IET Commun.* 4(1), 116–124 (2010)
4. Ghobaei-Arani, M., et al.: An autonomous resource provisioning framework for massively multiplayer online games in cloud environment. *J. Net. Comput. Appl.* 142, 76–97 (2019)
5. Boulogeorgos, A.-A.A., et al.: Effects of RF impairments in communications over cascaded fading channels. *IEEE Trans. Veh. Technol.* 65(11), 8878–8894 (2016)
6. Badarneh, O.S., et al.: Ratio of products of fluctuating two-ray variates. *IEEE Commun. Lett.* 23(11), 1944–1948 (2019)
7. Du, H., et al.: On the distribution of the ratio of products of Fisher-Snedecor F random variables and its applications. *IEEE Trans. Veh. Technol.* 69(2), 1855–1866 (2020)
8. Ghobaei-Arani, M., et al.: ControCity: An autonomous approach for controlling elasticity using buffer management in cloud computing environment. *IEEE Access* 7, 106912–106924 (2019)

9. Badarneh, O.S., et al.: Product and ratio of product of Fisher-Snedecor \mathcal{F} variates and their applications to performance evaluations of wireless communication systems. *IEEE Access* 8, 215267–215286 (2020)
10. Leonardo, E.J., et al.: The ratio of independent arbitrary $\alpha - \mu$ random variables and its application in the capacity analysis of spectrum sharing systems. *IEEE Commun. Lett.* 16(11), 1776–1779 (2012)
11. Karagiannidis, G.K., et al.: N^* Nakagami: A novel stochastic model for cascaded fading channels. *IEEE Trans. Commun.* 55(8), 1453–1458 (2007)
12. Lu, H., et al.: Accurate approximation to the PDF of the product of independent Rayleigh random variables. *IEEE Antennas Wireless Propagat. Lett.* 10, 1019–1022 (2011)
13. Chen, Y., et al.: Novel approximations to the statistics of products of independent random variables and their applications in wireless communications. *IEEE Trans. Veh. Technol.* 61(2), 443–454 (2011)
14. Annavajjala, R., et al.: On a ratio of functions of exponential random variables and some applications. *IEEE Trans. Commun.* 58(11), 3091–3097 (2010)
15. Nadarajah, S., Kotz, S.: On the product and ratio of Gamma and Weibull random variables. *Economet. Theory* 22(2), 338–344 (2006)
16. Sagias, N.C., Tombras, G.S.: On the cascaded Weibull fading channel model. *J. Franklin Inst.* 344(1), 1–11 (2007)
17. Carter, B.D., Springer, M.D.: The distribution of products, quotients and powers of independent H -function variates. *SIAM J. Appl. Math.* 33, 542–558 (1977)
18. Leonardo, É.J., Yacoub, M.D.: The product of two $\alpha - \mu$ variates and the composite $\alpha - \mu$ multipath-shadowing model. *IEEE Trans. Veh. Technol.* 64(6), 2720–2725 (2015)
19. Bhargav, N., et al.: On the product of two $\kappa - \mu$ random variables and its application to double and composite fading channels. *IEEE Trans. Wireless Commun.* 17(4), 2457–2470 (2018)
20. Leonardo, E.J., Yacoub, M.D.: Product of $\alpha - \mu$ variates. *IEEE Wireless Commun. Lett.* 4(6), 637–640 (2015)
21. Kong, L., et al.: Cascaded $\alpha - \mu$ fading channels: Reliability and security analysis. *IEEE Access* 6, 41978–41992 (2018)
22. Da Silva, C.R.N., et al.: Product of two envelopes taken from $\alpha - \mu$, $\kappa - \mu$, and $\eta - \mu$ distributions. *IEEE Trans. Commun.* 66(3), 1284–1295 (2017)
23. Badarneh, O.S., da Costa, D.B.: Cascaded fluctuating two-ray fading channels. *IEEE Commun. Lett.* 23(9), 1497–1500 (2019)
24. Silva, H. S., et al.: Cascaded double Beaulieu-Xie fading channels. *IEEE Commun. Lett.* 24(10), 2133–2136 (2020)
25. Leonardo, É.J., et al.: Ratio of products of $\alpha - \mu$ variates. *IEEE Commun. Lett.* 20(5), 1022–1025 (2016)
26. Da Silva, C.R.N., et al.: Ratio of two envelopes taken from $\alpha - \mu$, $\kappa - \mu$, and $\eta - \mu$ variates and some practical applications. *IEEE Access* 7, 54449–54462 (2019)
27. Mathai, A.M.: Products and ratios of generalized gamma variates. *Skandinavisk Aktuarietidskrift*, pp. 193–198 (1972)
28. Kong, L., et al.: Unified framework for secrecy characteristics with mixture of Gaussian (MoG) distribution. *IEEE Wireless Commun. Lett.* 9(10), 1625–1628 (2020)
29. Zedini, E., et al.: Performance analysis of dual-hop underwater wireless optical communication systems over mixture exponential-generalized gamma turbulence channels. *IEEE Trans. Commun.* 68(9), 5718–5731 (2020)
30. Atapattu, S., et al.: A mixture gamma distribution to model the SNR of wireless channels. *IEEE Trans. Wireless Commun.* 10(12), 4193–4203 (2011)
31. Al-Hmood, H., Al-Raweshidy, H.S.: Unified modeling of composite $\kappa - \mu$ /gamma, $\eta - \mu$ /gamma, and $\alpha - \mu$ /gamma fading channels using a mixture gamma distribution with applications to energy detection. *IEEE Antennas Wirel. Propag. Lett.* 16, 104–108 (2017)
32. Al-Hmood, H., Al-Raweshidy, H.S.: Unified analysis of channel capacity under different adaptive transmission policies. *Electronics Lett.* 56(2), 87–89 (2020)
33. Al-Hmood, H., Al-Raweshidy, H.S.: Unified approaches based effective capacity analysis over composite $\alpha - \eta - \mu$ /gamma fading channels. *Electronics Lett.* 54(13), 852–853 (2018)
34. Lei, H., et al.: Performance analysis of physical layer security over generalized- K fading channels using a mixture Gamma distribution. *IEEE Commun. Lett.* 20(2), 408–411 (2016)
35. Kong, L., Kaddoum, G.: Secrecy characteristics with assistance of mixture Gamma distribution. *IEEE Wireless Commun. Lett.* 8(4), 1086–1089 (2019)
36. Jung, J., et al.: Capacity and error probability analysis of diversity reception schemes over generalized- K fading channels using a mixture gamma distribution. *IEEE Trans. Wireless Commun.* 13(9), 4721–4730 (2014)
37. Al-Hmood, H., Al-Raweshidy, H.S.: On the sum and the maximum of non-identically distributed composite $\eta - \mu$ /gamma variates using a mixture Gamma distribution with applications to diversity receivers. *IEEE Trans. Veh. Technol.* 65(12), 10048–10052 (2016)
38. Chauhan, P.S., et al.: On the physical layer security over Beaulieu-Xie fading channel. *Inter. J. Electron. Commun. (AEU)* 113, 152940–152947 (2020)
39. Beaulieu, N.C., Jiandong, X.: A novel fading model for channels with multiple dominant specular components. *IEEE Wireless Commun. Lett.* 4(1), 54–57 (2015)
40. Papazafiroopoulos, A.K., et al.: The $\alpha - \lambda - \eta - \mu$: a general fading distribution. *Proceedings of IEEE Wireless Communications and Networking Conference*, pp. 1–6. IEEE, Piscataway (2009)
41. Mathai, A.M., et al.: *The H-Function: Theory and Applications*. Springer Science & Business Media, New York (2009)
42. Gradshteyn, I.S., Ryzhik, I.M.: *Table of Integrals, Series and Products*, 7th ed. Academic Press Inc., Burlington (2007)
43. Bodenschatz, C.D.: Finding an H -function distribution for the sum of independent H -function variates. Ph.D. Dissertation, The University of Texas at Austin (1992).
44. Abramowitz, M., Stegun, I.A.: *Handbook of Mathematical Functions: With Formulas, Graphs, and Mathematical Tables*. Dover, New York (1965)
45. Simon, M.K., Alouini, M.-S.: *Digital Communication Over Fading Channels*, 2nd ed. Wiley, New York (2005)
46. Celia, G.-C., et al.: Capacity of $\kappa - \mu$ shadowed fading channels. *Int. J. of Antennas and Propagation* 2014, 975109 (2014)
47. Wolfram Research, Inc. Available: <http://functions.wolfram.com/id> (2020). Accessed May 2020
48. Wu, D., Negi, R.: Effective capacity: A wireless link model for support of quality of service. *IEEE Trans. Wireless Commun.* 2(4), 630–643 (2003)
49. Al-Hmood, H., Al-Raweshidy, H.S.: On the effective rate and energy detection based spectrum sensing over $\alpha - \eta - \kappa - \mu$ fading channels. *IEEE Trans. Veh. Technol.* 69(8), 9112–9116 (2020)
50. Atapattu, S., et al.: Analysis of area under the ROC curve energy detection. *IEEE Trans. Wireless Commun.* 9(3), 1216–1225 (2010)
51. Al-Hmood, H., Al-Raweshidy, H.S.: Performance analysis of physical-layer security over fluctuating Beckmann fading channels. *IEEE Access* 7, 119541–119556 (2019)

How to cite this article: Al-Hmood H, Al-Raweshid H. Ratio of products of mixture gamma variates with applications to wireless communications systems. *IET Commun.* 2021;15:1963–1981.
<https://doi.org/10.1049/cmu2.12228>